

UNCLASSIFIED

AD NUMBER
AD826301
NEW LIMITATION CHANGE
TO Approved for public release, distribution unlimited
FROM Distribution authorized to U.S. Gov't. agencies and their contractors; Administrative/Operational Use; DEC 1967. Other requests shall be referred to Space and Missile Systems Organization, Los Angeles, CA.
AUTHORITY
SAMSO ltr, 28 Feb 1972

THIS PAGE IS UNCLASSIFIED

AD826301

TECHNICAL INFORMATION SERIES

AD 826301

THE IONIZED FLOW FIELD
OVER RE-ENTRY BODIES

SPACE SCIENCES
LABORATORY

BEST AVAILABLE COPY

SPACE SCIENCES LABORATORY

THE IONIZED FLOW FIELD OVER RE-ENTRY BODIES*

by

H. G. Lew

CLASSIFICATION: UNCLASSIFIED

This document is subject to the controls and each transmittal to foreign nationals may be made only with prior approval of SAMSO/SMSD

L.A. AFS / L.A. Policy 90045

Presented at the Conference on the Application of Plasma Studies to Re-Entry Vehicle Communications, October 3-4, 1967. U.S. Air Force Avionics Laboratory and Ohio State University.

*This work was supported by Air Force Space and Missile System Organization, Contract F04 694-67-C-0052.

R67SD70

December 1967

MISSILE AND SPACE DIVISION

BEST AVAILABLE COPY

GENERAL  ELECTRIC

TABLE OF CONTENTS

	PAGE
LIST OF FIGURES	iii
SUMMARY	1
I. INTRODUCTION	2
II. THEORETICAL ANALYSIS	6
A. LAMINAR BOUNDARY LAYER	6
B. INVISCID NONEQUILIBRIUM FLOW	9
C. STAGNATION REGION OF BLUNTED BODIES	11
III. RESULTS AND DISCUSSION	13
A. STAGNATION REGION	13
B. NOSE BLUNTNESS EFFECT ON ELECTRON DENSITY DISTRIBUTION	18
C. STAGNATION MARTIAN ATMOSPHERE	22
D. MASS TRANSFER OF ABLATION MATERIAL (Hydrocarbon, Graphite, Alkali Metal, Teflon)	23
IV. CONCLUDING REMARKS	28
REFERENCES	30
TABLES	31
FIGURES	36

LIST OF FIGURES

	PAGE
Figure 1 Blunt Conical Body	36
Figure 2 Variation of Axial Pressure Gradient Across Layer	36
Figure 3 Electron Density Variation Across Viscous Layer for Variable β	37
Figure 4 Oxygen Concentration, Stagnation Point	37
Figure 5 NO^+ , Stagnation Point	38
Figure 6 Temperature and Velocity Variation Across Viscous Layer, 250,000 ft.	38
Figure 7 Mass Fraction of Oxygen Molecule Across the Viscous Layer, 250,000 ft.	39
Figure 8 Positive-Ion Distribution Across Viscous Layer, 250,000 ft.	39
Figure 9 Stagnation Point Electron Density At Boundary Layer Edge	40
Figure 10 Temperature and Velocity Variation Across Viscous Layer, 200,000 ft.	40
Figure 11 Species Distribution Across Viscous Layer, 200,000 ft.	41
Figure 12 Velocity at Edge of Boundary Layer	41
Figure 13 Temperature Along Body	42
Figure 14 Pressure and Velocity Distribution Along Outer Edge of Boundary Layer	42
Figure 15 Temperature Distribution Along Outer Edge of Boundary Layer	43
Figure 16 Atomic O and N Distribution Along Outer Edge of Boundary Layer	43
Figure 17 Pressure Distribution Along Inviscid Streamlines	44
Figure 18 Peak Mass Fraction of Species Along Body	44

LIST OF FIGURES

	PAGE
Figure 19 Peak Electron Density on Blunt Cones	45
Figure 20 Maximum Electron Density Distribution	45
Figure 21 Mass Fraction of Species Across the Boundary Layer	46
Figure 22 Velocity Profiles with Injection of Pyrolysis Gases	46
Figure 23 Temperature Profiles with Injection of Pyrolysis Gases	47
Figure 24 Mass Fraction Profiles with Injection of Pyrolysis Gases	47
Figure 25 Maximum Mass Fraction Profiles With Injection of Pyrolysis Gases	48
Figure 26 Electron Density for Hydrocarbon - Air Boundary Layer	49
Figure 27 Mass Flux into the Boundary Layer for Graphite Oxidation	50
Figure 28 Mass Fraction of Species at Wall	50
Figure 29 Maximum Temperature in the Boundary Layer	51
Figure 30 Maximum Electron Density	51
Figure 31 Peak Electron Density with Seeding	52

SUMMARY

The prediction of communication through the ionized flow field about a re-entry body requires the knowledge of the detailed distribution of electron density. In this paper, recent studies at GE aimed at these predictions by analysis are presented. Results are presented for obtaining the characteristics of the chemically reacting boundary layer and viscous layer with finite reaction rates on sharp and blunt conical re-entry vehicles with the inclusion of the effects of mass transfer from ablation products and surface reactions. The equations have been formulated into a system of finite difference equations and a computer program to study the various phenomena that can influence the electron density in the flow has been developed. It is found that the effect of a small bluntness at the nose creates a dominant number of electrons and these effects of a small nose radius on re-entry body characteristics and electron density are discussed and comparisons are made with those of a sharp cone. In addition, the results of this investigation discussed herein include the effects of alkali metal seeding, mass transfer of hydrocarbon ablation products, and catalytic surface characteristics on the electron density distributions.

I. INTRODUCTION

Re-entry communication depends to a large extent on the penetration of an electromagnetic signal through the ionized flow field which envelops the body. It is known that the prediction of the attenuation of a small amplitude electromagnetic signal can be estimated reasonably well if the electron density distribution is known.

In this paper, some recent studies at GE on the prediction of the electron density distribution about re-entry bodies will be presented. At hypersonic speeds, shock layer temperatures are sufficiently high to dissociate and ionize the air. The electron density in these ionized layers have widely varying concentrations of electrons dependent on the flight velocity, altitude, and vehicle configuration. The determination of these electron concentrations is a complex problem in chemically reacting gas dynamics since finite rate chemistry is involved at the altitude of concern. Theoretical studies must include a multicomponent chemically reacting boundary layer and viscous layer over sharp bodies, slightly blunted bodies, and stagnation region of very blunt bodies, and in addition, must include the ionized and dissociated air species, the ablation products from hydrocarbon species, sodium, teflon species and their reaction with the air species and each other. Surface reactions for recombination of the atomic species and for graphitic bodies are also significant. Moreover, mass transfer from ablation products such as charring plastic ablators and teflon material must be taken into account with nonequilibrium and finite rate chemistry over most of the altitude region. These considerations have been integrated into a study which has culminated in the development of a finite difference method and a computer code which allows the inclusion of multicomponent diffusion with as many as 25 species with realistic transport and thermodynamic properties to evaluate the detailed distribution of electron

density over the bodies mentioned above.

Electrons are created in the gas phase primarily by air species and the ablation species. For a clean air flow over a sharp cone, the production of electrons is due primarily to viscous dissipation and increases with downstream distance along the cone. The effect of altitude and velocity with a comparison of results utilizing various rates suggested in the literature is discussed for sharp cones. Most bodies have some non-zero bluntness at the nose so that a stagnation region is created at the tip. The effect of this bluntness in the production of electrons is large. It is shown that for a slightly blunted cone the dominant electron production occurs at the nose of the vehicle and the subsequent behavior of the electrons downstream is a decay in contrast to the rise for the sharp cone. It is shown that the distribution of electrons around a slightly blunted cone and sharp cone do approach each other asymptotically downstream but only at a very large distance. For the slightly blunted cone, the edge of the boundary layer receives flow from different parts of the bow shock, i.e., the nonequilibrium inviscid flow is swallowed into the boundary layer. In other words, the boundary layer edge condition is not that of the stagnation streamline. The effect of the different edge conditions is discussed and examples are shown.

Mass transfer of ablation species into the boundary layer has a large effect. In addition to the change of gross characteristics such as temperature and velocity within the layer, the mass transfer of material species into the boundary layer leads to many more reactions with the air species. For most bodies there are surface reactions of air species with the body material. In particular, the ablation of graphitic bodies is due entirely to this process and there is also catalytic-recombination of atomic species at the surface. Results are shown for these cases and their effect on

electron production. Increases of the electron production by the minor material species in chemi-ionization processes are possible. Quenching of the electron production due to the lowering of temperature by the cooling effect of transpiration gases is also possible. Results for the injection of hydrocarbon species, i. e., pyrolysis gases, into the boundary layer with the additional homogeneous reaction with air are given and the effect on electron production is evaluated. Some results for the addition of teflon species are shown. In particular, the efficiency of the process of the attachment of electrons to fluorine atoms as a means of electron consumption is shown. The presence of sodium in the boundary layer and the subsequent increase of electron density is also investigated. These results have some significance in the problem of the addition of electronegative species to change the electron density level.

At the stagnation point, the nonequilibrium effects appear where the flow is mostly viscous. In other words, the entire boundary layer fills the distance between the shock and body. Results for a viscous layer theory with chemical activity of species at finite reaction rates have been obtained. These results extend through the merged layer region and are valid almost to the end of the continuum range of altitude. By studying the results for several cases, it is shown that the viscous shock layer forms a divided inviscid and boundary layer with the decrease of altitude. The production of electrons at the higher altitudes is shown.

In the next sections, the analysis that has developed in this study is discussed with emphasis on the physical assumptions considered. Next, results of the electron density distribution, slightly blunted bodies, stagnation region, and sharp nose bodies are given for hypersonic re-entry. It will be seen that the electrons are due to a combination of fluid mechanics phenomena as mass transfer, diffusion, and viscous

dissipation and of chemical reactions.

This paper contains the main results drawn from reports by F. G. Blottner and the author with some additional new results. Details of the equations and methods of computation are given in Refs. (3) and (4). It is a pleasure to acknowledge the contribution of F. G. Blottner to the work reported herein. A debt of gratitude is owed to the following. The chemical reactions and rates are those recommended by W. G. Browne, M. Bortner, W. Kaskan, and R. Porter. The computer programming and results were competently obtained by Mrs. Susan Kendall and Miss Sindy Dectrow. The typing and preparation of the manuscript was carefully done by Mrs. Terry Spence. Several illuminating discussions have been held with R. Porter on chemi-ionization mechanisms of high temperature hydrocarbon and air reactions.

II. THEORETICAL ANALYSIS

The purpose of this paper is the prediction of electron density distribution over re-entry bodies for sharp cones and slightly blunted cones. This would include the consideration of the stagnation region of blunt bodies. The altitudes of concern here varies from 300,000 ft. to about 50,000 ft. where equilibrium flow will then prevail over these bodies. It is sufficient to treat the flow as laminar as this state of the gas is dominant down to about the latter altitude for the re-entry velocities of concern. These velocities are of the order of 20,000 ft/sec. For these conditions, the chemical state of the gas is a nonequilibrium one and the kinetic energy transformation into thermal energy immediately leads to a highly dissociated and ionized air species. In the case of planetary entry $\text{CO}_2 - \text{N}_2$ species are involved and the altitudes and velocities for significant nonequilibrium are changed accordingly. It is expected that a high degree of nonequilibrium will exist even for lower altitudes in Martian entry and tends toward equilibrium in the Venus atmosphere because of the higher density.

A. LAMINAR BOUNDARY LAYER

The equations of motion involved are those for a laminar boundary layer development over an axially symmetric body with an arbitrary meridian shape. For nonequilibrium flow with multicomponent transport phenomena, these equations are given in Ref. (1). Since a narrow region next to the body is of concern, the more general equation reduces to the boundary layer form; this leads to the deletion of the second derivatives with respect to streamwise direction terms. Surface coordinates are used with one coordinate along the surface measured from the stagnation region of the blunted cone or from the tip of a sharp cone as the case may be. These equations

are those for the conservation of axial momentum, energy, and species with the addition of the equation of state. Momentum conservation in the direction normal to the body is usually small consistent with high Reynolds Number boundary layers and this equation is not considered except for the low Reynolds stagnation region considered in Section C. For a real gas behavior, the thermodynamics properties of enthalpy and specific heats of the individual species are used. The multicomponent transport properties as viscosity and thermal conductivity of the mixture are obtained by Wilke's formula from individual specie properties with the latest literature values of the collision integral. Multicomponent diffusion are also considered with ambipolar diffusion of the ions and electrons.

The basic gas model for re-entry into the earth's atmosphere involves the species O_2 , N_2 , O , N , NO , NO^+ and electrons for velocities to about 20,000 ft/sec. In addition, the ablation of material into the boundary layer leads to many other hydrocarbon, sodium, and teflon species which forms other compounds due to reaction with the dissociated and ionized air. Homogeneous reactions of these species are taken into account. The kinetic rates for these processes and the reactions considered in this paper are given in Tables I and II.

The equations of motion for the transport phenomenon as described are highly nonlinear partial differential equations with the surface coordinates as independent variables. The number of these equations can be as large as 26 with the unknowns of velocity components, temperature, and species. The method of solution selected is that of implicit finite differences of the Crank-Nicolson type. Stable solutions with sufficiently large step sizes are obtained by this method so that a boundary layer development over a typical body can be obtained within a reasonable computer time.

The formulation of the implicit difference scheme leads to a system of linear algebraic equations which are tri-diagonal and can be solved by a sweeping technique. Iterative calculation of the coefficients when necessary usually assures the convergence of the method for a given step size.

The boundary condition for these equations depend to a large extent on the behavior of the surface material and the body geometry. The surface conditions are described in this section. At the surface, the heat transfer can be considered for either a fully catalytic or a noncatalytic material. It is necessary to formulate these conditions for a multicomponent mixture of gases. For the cases where the ablation of surface material occurs, the surface condition includes the mass transfer normal to the surface. The complication to the solution of the equations is not only at the surface but also in the interior of the boundary layer where an inflected velocity profile and larger displacement thickness are obtained. In addition, the usual conditions of the vanishing of the tangential velocity component at the surface and of either a prescribed wall temperature or adiabatic wall are made.

At the outer edge of the boundary layer flow over conical bodies or high Reynolds Number flow at the stagnation point, the inviscid body streamline leads directly to the boundary conditions for the velocity, temperature, and species concentrations. For slightly blunted bodies, the boundary layer will swallow fluid from inviscid streamlines processed through the bow shock other than that of the stagnation region. Since the inviscid flow for these streamlines are usually in nonequilibrium, it is necessary to integrate the inviscid equation from the shock to the edge of the boundary layer. This consideration of the inviscid nonequilibrium computation is relegated to the next section.

Besides the boundary conditions, this system of equations is parabolic and initial

conditions are required to completely specify the solution. For these conditions, the equations of motion are first reduced to the limiting forms at the tip of the sharp cone or at the stagnation point. This reduction leads to ordinary differential equations with two-point boundary conditions which are solved by finite difference methods. These equations involve the same thermodynamics and transport properties as above. Some additional remarks will be made for the stagnation point in Section C. With these initial conditions, the finite difference method then allows the solution to be obtained in a step-by-step procedure marching downstream.

B. INVISCID NONEQUILIBRIUM FLOW

For the determination of the conditions at the outer edge of the boundary layer for a sharp nose body, it is sufficient to integrate the inviscid equation along the body streamline. The body pressure distribution is prescribed and may be that given from experimental measurement or inviscid flow field computation. Usually, it is found that the conditions along the edge do not change much along the surface of a sharp nose body; that is, only a negligible amount if dissociation or ionization is present.

For a slightly blunted conical body, the different inviscid streamlines entering the successive points of the boundary layer edge has passed through different points of the bow shock. The chemical state along each of these streamlines are, therefore, different. In general, different nonequilibrium state exists for each streamline de-pendent to a large extent on the initial point where the streamline pierces the bow shock. Several methods have been used to obtain the development of the characteristics along the streamlines. They differ in the manner in which the pressure distribution is accounted for. These methods have included pressure variation across the inviscid shock layer and the pressure overexpansion. The method of obtaining the inviscid

conditions follows next.

The appropriate swallowing of the inviscid fluid into the boundary is considered by first determining the corresponding points at the bow shock wave and boundary layer edge which have equal mass flux. It is supposed that an estimate of the boundary layer edge location is available. These points are then the initial and end points of the various streamlines. Since it is known that pressure distributions of the flow are not changed appreciably by nonequilibrium effects, these distributions can be taken from equilibrium flow fields. This can be done by three different methods. In method A, the pressure gradient immediately behind the shock is utilized for the gradient along each streamline. This implies that the same pressure gradient is assumed for each streamline and the pressure gradient normal to surface is zero which is not unreasonable for a slightly blunted conical body. In a second method, B, the pressure gradient along the streamline is determined by an approximate integration of the normal pressure gradient across the inviscid shock layer. This is done in stream function coordinates. In this way, pressure overexpansion is accounted for. Pressure distributions obtained in this way have been shown to be an excellent approximation to the inviscid flow field. A third method, C, has also been considered. The complete pressure field from a numerical solution of the equilibrium inviscid flow field (G. E. program) has been utilized for the pressure distribution of each inviscid streamline. The location of each streamline and shock shape from this solution are also used. Pressure overexpansion along the body are, of course, taken into account.

These assumed pressure gradient then allows the solutions of the streamtube inviscid nonequilibrium equations to be obtained. In general, velocity, temperature, and air species are found along the streamline and at the edge of the boundary layer.

With the new edge conditions, the boundary layer flow characteristics is determined and a new distribution of boundary layer mass flux is obtained. This new mass flux then leads to new edge conditions and iterations are performed until the mass flux do not change appreciably.

C. STAGNATION REGION OF BLUNTED BODIES

Initial conditions are required for the unique solutions of the system of equations discussed in Section A. Since the Mangler-Howarth-Dorodnitsyn transformation is utilized herein, the density does not appear explicitly in the equations; and moreover, the transformation leads to the correct form of the equations at the tip of a sharp nosed body (or at the stagnation point of a blunt body) if the limiting process of allowing the streamwise variable to approach zero is made. Thus, the initial condition for either types of noses are ordinary differential equations which are two-point boundary value problems. These are usually difficult to solve by the more common method of "shoot and hunt" since so many specie are considered; they are solved here by the application of finite difference methods so that the two end conditions are always satisfied. The resulting algebraic equation from the finite difference formulation are tridiagonal and a sweeping method of solution is used. Iteration is then applied until successive profiles are sufficiently close to each other. The previous discussion applies to conditions of altitudes and velocity where the boundar, layer equations as discussed in Section A are valid. Considerations have also been given to flight conditions where this validity is violated. The development of the flow at stagnation area for these cases are given in the remainder of this section.

At the higher altitudes, nonequilibrium and viscous effects begin to have equal importance over the entire shock layer. This is dependent to a large extent on the nose

radius concerned, but the criterion of importance can be estimated by the product of the density and nose radius. For example, the boundary layer thickness is practically equal to the inviscid detachment distance for a 1/4" nose radius body at 150,000 ft. altitude traveling at 20,000 ft/sec. At this low Reynolds number range, a set of equations have been considered which is valid for the entire viscous layer at the stagnation point. Normal pressure gradient across the layer as far as centrifugal effects are concerned are taken into account. The boundary conditions are applied at the surface of the body and at the shock wave. At the shock, the effects of diffusion, heat transfer, and shear stress are accounted for. Estimates and later validation of these conditions are made by considering the set of equations in the shock transition zone. With these equations and boundary conditions, viscous nonequilibrium flow characteristics for the low Reynolds number range have been obtained.

A more detailed discussion of the development of these equations as outlined above are given in the reports by Lew² and Blottner.³

III. RESULTS AND DISCUSSION

The complete ionized flow field with finite rate chemistry of air and many ablation products for flow over blunted conical bodies have been studied by the method outlined in Section II. Some of these results pertinent to the re-entry vehicles communication problem will be discussed here.

A. STAGNATION REGION

For blunt nosed bodies, the stagnation region is of particular importance not only because the flow is initiated at this point but the nose is one of the principal mechanisms for producing electrons. In most cases, the maximum electron density occurs at this point and decays downstream. As discussed in Section II, the flow over small blunt noses are usually entirely viscous even down to altitudes of 100,000 ft. Thus, at the higher altitudes where the flow is entirely viscous in the stagnation region, the viscous equations at the stagnation region with tangential pressure gradient variation across the viscous layer yields the results in Figs. 2 to 5 for a 1/4" nose radius at an altitude of 200,000 ft. and velocity of 20,000 fps for air. The significant figure is number 3 which shows the electron density variation across the viscous layer from the body to the shock. The coordinate y in the figure is the actual physical distance. Results for two altitudes of 150,000 ft. and 200,000 ft. are shown. Even at 200,000 ft. an appreciable number of electrons of the order of 10^{10} electrons/cc are produced at the stagnation point.

For an order of magnitude increase in density from 200,000 ft. to 150,000 ft. altitude, the electron density has increased by about 3 orders. Much of this change is due to the higher dissociation of O_2 at the lower altitude. For the case given in these

figures, the frozen Rankine-Hugoniot shock conditions are applied at the shock. Since the composition is frozen as the flow passes through the shock, only oxygen and nitrogen molecules are present at this point and the translational temperature is high. Then the finite rate chemistry are initiated and the oxygen molecules begin the dissociation process. The concentration of oxygen molecules continues to decrease proceeding with the flow from the shock to the body; it achieves a minimum within the layer and then increases toward the body which is held at a constant wall temperature. The variation of mass fraction of positive ion NO^+ is shown in Fig. 5 consistent with the trend of the O_2 curve. It is noted that the ionization mechanism is the associative recombination of N and O atoms.

It would be useful to consider additional results under the same boundary condition at the shock for a larger body. These results are shown in Figs. 6, 7, and 8 for a body with a nose radius of 1.86 ft. traveling at a velocity of 21,600 ft/sec and an altitude of 250,000 ft. It is seen that the nose radius has been increased about 90 times from the previous case but with only smaller increases in velocity and altitude. However, the variation of the profiles are similar across the entire viscous layer. Fig. 6 shows the temperature and velocity profiles with η equal to zero at the body surface. The variable η is the density transformed distance across the layer and related in a nonlinear way to the physical distance y as given in Fig. 3. From Fig. 6 it is seen that there is a steep decrease in the temperature variation near the shock front which becomes more gradual inside the viscous layer; then there is a sharp decrease to the wall temperature. The steep portion of this variation is due to dissociation of the molecular species, for example, see Fig. 7. The temperature immediately aft of the shock front is $26,525^\circ\text{R}$ and the wall temperature is 1000°R .

This wall temperature is a reasonable one at the altitude under consideration. Additional boundary conditions for the body surface are needed for the species. For the cases under discussion, the condition for equilibrium composition at the prescribed wall temperature and pressure is utilized and is equivalent to that of a fully catalytic wall for heat transfer at this low wall temperature. The velocity profile U/U_E shown on Fig. 6 indicates a constant vorticity region near the shock. This suggests that a boundary layer model in which the boundary layer thickness is about one third of the physical detachment distance matched with an inviscid flow with constant vorticity in both the values of the velocity and its slope would be sufficient to predict the same results in flow characteristics. For this type of consideration, the boundary layer thickness would be about 0.02 times the nose radius and is still sufficiently small for boundary layer theory to be valid. The behavior of the species profile is similar to that of the case for the smaller nose radius. Due to the high translational temperature near the shock, oxygen atoms are created by dissociation of O_2 through reaction (1) with a small contribution from the dissociation of NO; the principal loss of O atoms near the shock is by means of the shuffle reaction. Further in the layer towards the body, oxygen atoms are still being produced but now a contribution is added by the shuffle reaction instead of a loss and the net production continues until the body surface is reached. In contrast, nitrogen atoms are present in the region near the wall due principally to diffusion from the upper layers. The maximum production of atomic species occurs at a distance of about 1/3 of the detachment distance from the body and drops to zero at the wall. Equilibrium composition at the wall contains only the molecular species. If the other extreme of surface condition of a noncatalytic one is assumed, the peak atomic concentrations would continue to the wall. The concentration of nitric oxide

is shown on Fig. 8 and it is produced near the shock primarily by the bimolecular shuffle reactions 4 and 5 with about a small amount used in the production of N and O atoms by dissociation reaction 3. The loss of NO near the wall is due to reaction 5 in the production of oxygen atoms. Although there are two positive ions considered in the results for the body with larger nose radius, the principal contributor to the electron density at this velocity is that due to NO^+ . NO^+ is produced in the upper layers of the flow near the shock and consumed in the lower layer; diffusion of the species occurs toward both ends. Values of the electron density of the order of 10^{12} no./cc are obtained; the maximum of 7.2×10^{12} no./cc is at about 1/3 of the distance from the body surface.

Results have also been obtained for several other conditions. Details may be found in Ref. 2. At the lower altitude of 200,000 ft., the formation of a thin boundary layer is more accentuated (Fig. 10). The temperature distribution reveals an interesting variation. There is a step drop in temperature at both ends of the viscous layer separated by an almost constant temperature zone occupying about 70% of the viscous layer. In the layer with an extent of 15% of the detachment distance from the body surface, the shuffle reactions are very rapid and near equilibrium conditions prevail. Species are shown in Fig. 11. Electron density of the order of 10^{13} electrons/cc is obtained at this altitude. It is noted that since part of the layer is near equilibrium it is possible for the altitude and nose radius considered that collisional ionization of N and O atoms might be important in the production of electrons. Equilibrium conditions at the density and temperature inside the viscous indicate large amounts of N^+ and O^+ .

For the higher altitude regime, the Reynolds Number based on the nose radius becomes sufficiently low so that the heat transfer, diffusion, and shear stress may modify the Rankine-Hugoniot shock relations. In that case, a shock transition zone may

also appear since the shock wave may have a nonzero thickness. Results based on this type of model have been obtained and are given by Lew elsewhere.

Boundary Layer

At the low altitudes, the flow indicate a boundary layer region formation near the body which is small in extent compared to the nose radius. Moreover, equilibrium conditions exists in the inviscid flow outside this boundary layer. Due to this fortunate circumstance, the edge conditions for the boundary layer may be considered in equilibrium and the maximum ionization occurs at this edge. For this regime, the usual boundary layer equations as discussed in Section I with inviscid equilibrium flow fields (eg. GE or NASA) giving the edge conditions are sufficient. One notes that the flow in the interior of the viscous region still has nonequilibrium chemical activity. A large number of results have been obtained for this condition; it suffices to summarize the maximum electron density which occurs at the edge of the boundary layer in Fig. 9. By the boundary layer theory, the electron density profile is almost constant throughout the layer except near the wall where it drops to the surface condition. For a low wall temperature, the surface value is zero.

From the values of the electron density obtained in this section, it is clear that nose bluntness produces a significant number of electrons in the stagnation region even though only air species are present. The addition of ablation species can alter this; but usually only the alkali metal (or chemi-ionization processes) can increase these numbers appreciably. The behavior of the electron density variation downstream depends now not only on the values at the stagnation point, but also on the flow through the bow

shock, the influence on the production of additional electrons by viscous heating, and the catalytic wall condition. This is considered further in the following sections.

B. NOSE BLUNTNESSEFFECT ON ELECTRON DENSITY DISTRIBUTION

It has been shown in the previous section that large electron density concentrations are obtained at the stagnation point of a blunt body. For a slightly blunted body, the flow development along the conical portion of the body is complicated by the fact that flow through the different parts of the bow shock wave enter the boundary layer edge. A mixing of the streamlines with different entropy by diffusion and convection then occurs as the boundary layer grows along the surface of the body. The boundary layer edge conditions are obtained as discussed in Section II. All three methods have been used in obtaining these edge conditions. These results are shown in Figs. 12-17 for a slightly blunted 10° cone with nose radius of $1/4''$. An example of the different inviscid velocity distributions at the boundary layer edge utilizing either the body streamline pressure distribution or the matching of the flow mass flux at each point of the boundary layer edge with the corresponding inviscid streamline is shown on Fig. 12. The Newtonian pressure inviscid velocities are always slightly lower. However, even this small difference is significant in the region near the stagnation point. Temperature distribution at the boundary layer edge are composed with the body streamline values using the Newtonian pressure distribution in Fig. 13. The larger difference in the stagnation region is again significant because the temperatures are much higher. For the case considered (150,000 ft.), the boundary layer edge is close to the shock near the stagnation region as discussed previously; thus, the temperature is much higher than the equilibrium values. The temperature distribution immediately behind the bow shock is also shown in

this figure for comparison. It is reasonably close to the matched flux value. The remaining curve is the peak temperature distribution within the boundary layer. In these results, the pressure distribution required for the matched flux computation has been assumed to be that directly behind each point of the shock. Thus, the pressure is constant along the conical portion of the body. For this body, the cone-sphere junction is at a value of $x = .029$ ft. where x is the surface distance along the body measured from the stagnation point; x is the abscissa in these figures. However, for the family of sphere cone bodies there usually is a pressure overexpansion (as indicated by the dotted curve and crosses in Fig. 14) before the conical pressures are achieved along the body. Moreover, the pressure history of the individual streamlines are different than that along the shock or along the body. For these reasons, two other methods have also been employed in accounting for these deficiencies. These are discussed next.

Pressure variation across the inviscid shock layer has been taken into account by a closed form integration of the transverse momentum equation in stream function coordinates. This allows the pressure overexpansion to be accounted for with a different pressure distribution for each streamline; Fig. 14 shows the effect of the new pressure distribution on the inviscid velocity at the boundary layer edge (dash curve lines). It is evident from the figure that pressure overexpansion does not change the boundary layer edge velocity appreciably. Temperature and species distributions (dash curve) at the boundary layer edge are slightly below those using the body streamline (Figs. 15 and 17). The atomic species are shown since their presence can significantly alter the electron distribution. It may be pointed out that these values agree with the chemical reacting inviscid characteristic solutions of Cornell Aeronautical Laboratory.

For a more complete determination of the inviscid edge conditions, the third method utilizes the complete equilibrium inviscid flow field pressure to determine the edge conditions. The GE equilibrium inviscid flow field gives directly each streamline pressure and its physical location with respect to the body. Pressure distribution along streamlines are shown on Fig. 17. Pressure overexpansion is, of course, contained in these properties which can be also seen from Fig. 17. The coordinate X is the axial distance along the body. The shock shape used corresponds also to that determined as part of the equilibrium flow field computation. With the pressure distribution prescribed in this way, the inviscid nonequilibrium streamtube equations lead immediately to the results (crosses) shown on Figs. 14 to 16. Again, even with more correct equilibrium pressure and an overexpansion slightly below that used before, the velocity along the edge of the boundary layer is not appreciably different. However, the temperature distribution on Fig. 15 is below that predicted by the other two methods. This trend is also reflected in the species distribution where there is a more sudden drop of the atomic oxygen and nitrogen distribution. Since the bodies under consideration are only slightly blunted, the electron density behavior as the fluid passes through the boundary layer and interacts with the surface are more significant. In general, these methods of analysis of the inviscid nonequilibrium flow is sufficient for the purpose at hand. The sufficiency of the degree of approximation is determined to a large extent by their effect on the electron density decay in the boundary layer and by comparison with more accurate inviscid chemically reacting flows (which was pointed out above).

The electron density development in the boundary layer can now be determined using the edge conditions discussed above and the implicit finite difference for the nonsimilar equations. Results for the maximum values of the species and electron

density distributions along the body are shown on Figs. 18, 19, and 20. Equilibrium values of the species and electron density for conical conditions of temperature and pressure are indicated by the arrows on the right side of the figures. For the blunted cones, it is seen that maximum values of electron density and dissociated species as N and O are produced at the stagnation region and decreases to a minimum. Figure 18 shows that the gas species then increases and approaches asymptotically the values for a sharp cone and then both curves approaches the equilibrium values of these species at the conical temperature and pressure conditions. The sharp cone nonequilibrium creation of dissociated species and electrons is due primarily to heating of the fluid by viscous dissipation leading to a peak of temperature within the boundary layer which may be about 4 times the edge values. More elaborate results for sharp cone ionization have been obtained at GE and given in Ref. (3) utilizing an earlier computer program. Blotner has shown in Ref. (3) that the peak electron density is proportional to x^3 where x is the cone surface distance from the tip. In the case of the electron density distribution shown on Fig. 19, it is clear that even at 10 ft. downstream of the stagnation point that nowhere are the sharp cone values close to the blunted cone values. It is suggested by this comparison that short bodies with even a slight bluntness will have electron density entirely different from that of a sharp body. The effects of altitude change on the electron density are evident from Fig. 19 and is larger for sharp bodies at a given body location. Surface conditions can affect the electron density distribution through the loss of atomic species or temperature changes; the results for the two limiting conditions of a fully catalytic or noncatalytic surface with respect to the air species are shown here. A noncatalytic surface can increase the electron density if the body is sufficiently long.

The effect of using the different boundary layer edge conditions is shown on Fig. 20. These have been considered for the two methods of utilizing the pressure behind the shock and the approximate streamline pressure distribution. The electron density distributions determined in these ways are shown in Fig. 20. In the comparison, it should be kept in mind that stagnation region conditions are almost equivalent and the flow is fully viscous. The largest deviation in the two curves occurs between $x = 0.01$ to 0.1 where the outer edge conditions are most different. It is noted from the figure that at large distances from the nose the two distributions approach each other asymptotically as the conical pressure is slowly recovered. It is expected that the characteristics of the boundary layer for the boundary layer edge conditions given by the equilibrium flow field (crosses on Figs. 14 to 16) are close to that given by the approximate pressure distribution since the edge conditions are almost the same.

C. STAGNATION POINT - MARTIAN ATMOSPHERE

Atmospheric conditions for Mars appear to indicate that nonequilibrium effects will persist to even a lower altitude than for earth. Thus, even larger body size will pass through a longer nonequilibrium regime. The gas mixture is now CO_2 and N_2 . Results have been obtained for entry into this gas mixture to determine the nonequilibrium characteristics of the boundary layer at the stagnation point. The gas species was supposed to be made up of CO_2 , CO , N_2 , O_2 , O , N , and NO . An idea of the degree of ionization can be gotten from the variation of the atomic species O and N if the formation of the ion NO^+ is the only ion formed. The free stream conditions of $V_\infty = 14,000$ ft/sec, $\rho_\infty = 3.452 \times 10^{-7}$ slugs/ft³, $p_\infty = 0.086$ lb/ft² were used and a body with a nose radius of 4.75 ft. was considered. With a mixture of 60% CO_2 and 40% N_2 , the flow characteristics

prove to be highly nonequilibrium as shown in Fig. 21. Since the boundary layer forms at this altitude, the maximum values of the species concentrations occur at the edge of the layer. The boundary layer fills about a third of the detachment distance for this body.

D. MASS TRANSFER OF ABLATION MATERIAL

Hydrocarbon

The behavior of the boundary layer with mass injected at the surface of the body is considered here. In general, the boundary layer thickness is increased by the additional mass so that a cooler layer of fluid is formed next to the wall. In the case of flow over a sharp cone, it is remembered from the previous sections that viscous dissipation leads to a peak temperature (about 3 to 4 times the edge values) at a small distance from the surface. With the presence of mass transfer, this peak temperature is moved away from the wall. At the same time, the velocity profile acquires an inflection point. These points are illustrated by the results for injection of hydrocarbon gases into the boundary layer which would be typical of pyrolyzed gases from charring ablation material as phenolic-carbon. The example selected is a 9° sharp cone at 125,000 ft. altitude traveling at a velocity of 24,400 fps with a wall temperature of 1530°K. The total mass flux of species injected was considered constant along the surface and has a value of 2.2038×10^{-4} slug/ft² - sec. Results are summarized in Figs. 22 to 24 for the profiles of velocity, temperature, and species. The inflection in the velocity profile is evident in Fig. 22 and leads to a decrease in the viscous dissipation and hence a drop in downstream temperature; both effects are due to the mass transferred into the boundary layer. A drop in peak value of the temperature ratio T/T_e from 5.5 to 4.1 is shown on Fig. 23. One notes that there is a decrease in peak temperature

even in the presence of the combustion processes of hydrocarbon. Example profiles of the species concentration are given in Fig. 24. In general, the values at the wall ($\eta = 0$) corresponds to the values that were injected. The peak values on Fig. 25 shows that only nitrogen atom is approaching a constant asymptote. Electron density variation for this case is shown on Fig. 26 as compared to that of air. The principal air ionization mechanism included herein is that due to associative recombination of the N and O atoms. The electrons produced from chemi-ionization mechanisms of the hydro-carbon species are known to exist although the detailed processes are not sufficiently known at this point to be included in this analysis. However, Porter⁵ has suggested a phenomenological model for obtaining an estimate of the electron from hydro-carbon species. On the basis of correlation of experimental data, Porter has suggested that acetylene yields the H_3^+O ions in proportion to the hydroxyl radical concentration; the fraction of acetylene molecules oxidized to give ions decreases with increasing ratio of fuel to oxygen. By this means, the net production of H_3^+O ion can be obtained from the hydrocarbon-air boundary layer as discussed above. The distribution of electron density is shown on Fig. 26; an increase of several is evident. Porter has also suggested a similar means to obtain ion yield from methane. Porter's experimental work in progress will be able to improve this estimate in the near future.

Graphite

Graphite forms a class of material useful for protection of re-entry bodies. Exposure of this material to a hot air environment leads to ablation primarily through heterogenous reactions. Moreover, a carbonaceous char forms over material evolving hydrocarbon species and its surface material can be lost in a similar way. Thus, it

would be useful to consider in this section the nonequilibrium flow over graphite surfaces. Some of the homogeneous reactions for a $\text{CO}_2 - \text{N}_2$ atmosphere have been discussed previously. In addition, the species C, C_2 , and CN are considered. The results are considered here for the oxidation of the graphitic material by molecular oxygen. The surface temperature variation is assigned; it can, of course, be obtained from a heat balance with the surface material. With the experimental rate of material erosion known, the mass flux at the surface is obtained as part of the solution. Results for a 10° sharp cone at an altitude of 100,000 ft. traveling at a velocity of 22,000 ft/sec are shown on Figs. 27, 28, 29, and 30. The wall temperature is assumed constant with a value of 3000°K ; moreover, the air results for the comparison in Fig. 30 are for equilibrium composition at that temperature. Fig. 27 shows that the mass flux transferred into the boundary layer decreases downstream which is somewhat consistent with the trend shown by the mass fraction of oxygen molecules at the wall shown on Fig. 28. This figure also shows that atomic oxygen increases above the molecular oxygen from about 0.3 ft. downstream. Other results not shown here indicate that the inclusion of the atomic oxygen reaction with the carbon surface leads to an increase of mass loss along the surface in contrast to the decrease shown here since more atomic oxygen is available. For the flow considered here, the loss of surface material near the tip of the cone is reaction rate controlled since there is a large amount of oxygen available. Immediately downstream, the oxidation process becomes diffusion controlled and the mass flux decreases along the surface of the body. The peak temperature behavior shown in Fig. 29 indicates the effect of the mass transferred into the boundary layer near the leading edge of the cone; the peak temperature for the carbon-air boundary layer is less than that of air. Electron density are compared in Fig. 30 and

since the ionization mechanism is the same as for pure air, the decrease in the electron density of the graphite body is due principally to mass transfer effects via the temperature and to a smaller extent on the loss of oxygen to surface reaction.

Alkali Seeding in the Boundary Layer

It is well known that alkali contaminants as sodium added to the boundary layer can create a large number of electrons. For slender bodies, the reactions of sodium with air are in nonequilibrium. This case has been studied for air and the additional species of O^- , O_2^- , Na , Na^+ . Similar rates can be considered for Cs. A summary of these results of electron density for both sodium and cesium is shown on Fig. 31 for very small amounts of these elements. For the study, these elements are assumed to be included in the mass transferred during the ablation process. Thus, for the case considered of a 10° cone at 150,000 ft. altitude and at a velocity of 22,000 ft/sec. the mass flux was taken to be constant along the surface of the body; the mass flux of alkali metal to the total mass flux is as indicated. The remaining mass flux is taken to be nitrogen to represent the ablation products. Comparison with the pure air cone results indicate an increase of 4 to 5 orders of magnitude with sodium contaminants and a 7 to 8 orders of magnitude increase for cesium. The sodium is less than 0.5% ionized whereas the cesium is already 99% ionized. The most important reaction being the detachment process ($O_2 + e^- + M \leftarrow O_2^- + M$) for both sodium and cesium.

Teflon

The teflon-air boundary layer analysis provides some interesting results. For the study here it is supposed that C_2F_4 molecules are injected into the boundary layer. The mass rate transferred can, of course, be obtained from a material and heat

balance, but it is specified here. The mass flux injected varies along the cone surface with values of zero at the nose and a peak value of 10^{-4} slugs/ft² sec at $x = 0.1$ ft. and decaying asymptotically to zero (at $x = 5$ ft., it has a value of 3.16×10^{-5}). Even in the nonequilibrium situation considered here, the C_2F_4 injected rapidly dissociates to CF_2 away from the surface of the body. With the mass transfer of C_2F_4 , the effects on the boundary layer are two-fold. These are the fluid mechanical effects of cooling and diffusion causing the boundary layer to thicken and peak temperature to decrease along the body from 4.33 ($x=0$) to 4.18 ($x=5$ ft.) times the temperature at the edge of the boundary layer. Another is due to chemical effects. Some of this decrease temperature is due to the endothermic reactions, for example, one of the contributors of CF_2 and O_2 molecules (reaction (38)). A larger amount of O atoms are produced from the dissociation of O_2 molecules by CF_2 . The attachment processes of electrons to fluorine atoms are included in this kinetic scheme and given by reactions (43-44) in Tables I and II. Although there is large mass fraction of fluorine atoms present in the boundary layer which is of the order of the oxygen molecules, the mass fraction of negative fluorine ions is negligibly small. At $x \approx 2$ ft. downstream from the tip of the cone, the mass fractions of F^- and F are 1.79×10^{-12} and .038, respectively and at $x = 5$ ft. these values become 1.2×10^{-10} and .0828. These are the peak values across the boundary layer. The results indicate the flow is in a nonequilibrium state and not close to equilibrium at all. These results are based on a tentative chemical kinetic scheme. Experimental work underway in this laboratory will assist in the delineation of the proper scheme for this combination of gases.

IV. CONCLUDING REMARKS

Methods obtained at GE for the prediction of the electron density distribution about re-entry bodies have been discussed. These are based on detailed step-by-step integration of the equations of motions with chemistry utilizing finite difference techniques. A number of results have been shown for the electron density distribution subjected to effects of nose bluntness, ablation contamination, fluid injection, and surface reaction. The body materials considered have been the epoxy resins and Teflon yielding hydrocarbon and carbon-fluorine species, respectively. Flow over the stagnation region of blunt bodies, slightly blunted conical bodies, and sharp nose bodies are included for a wide range of Reynolds numbers. At low Reynolds Number, characteristics of the flow at the stagnation region of blunt bodies where the flow is entirely viscous have been also given in detail. The salient points in this prediction of electron density distribution are the following.

1. The nose bluntness is of essential importance in the production of electrons at the stagnation region and this effect persists for a long distance downstream. As a consequence, the electron density is much larger than that for a sharp cone, and are comparable to those created by chemical reactions with contaminant.
2. The viscous flow at stagnation regions produce large numbers of electrons even at the higher altitudes.
3. The effects of mass transfer due to the ablation of surface material are to form a cooler layer next to the wall and to displace the maximum temperature away from the wall. Reduction of the electron density can occur through the reduction in temperature.
4. The effect of hydrocarbon addition to the boundary layer with the ionization

due to associative ionization of N and O shows some changes in the electron density due to the chemical energy effects of reactions of the hydrocarbon-air species, i. e., the consumption of the injected species as methane and acetylene. Chemi-ionization mechanisms can produce large concentrations of electrons but more exact prediction will only be made when additional data on the particular mechanism is known.

5. The addition of sodium which is a material contaminant shows the large increase in electron density as expected; however, the study shows that the reactions are in nonequilibrium and most of the sodium introduced is ionized.

6. The addition of Teflon speices in air boundary layer indicates that loss of electrons in their attachment to fluorine atoms is not large in comparison with its production. It appears that further study must be made of the Teflon-air kinetic scheme.

7. Surface conditions of different catalytic efficiency can change the electron density significantly.

By means of this study, it is now possible to predict the detailed flow and chemical characteristics over typical re-entry bodies. In general, it has been shown that the electron density distribution is a sensitive function of body geometry and ambient conditions. It appears that much additional work is still needed, particularly, in the further delineation of the kinetic schemes for Teflon-air system, hydro-carbon-air system and their chemi-ionization mechanisms.

REFERENCES

1. Hirschfelder, J. O., Curtiss, C. F., and Bird, R. B., "Molecular Theory of Gases and Liquids", John Wiley and Sons, N. Y., 1954.
2. Lew, H. G., "The Distribution of Dissociated and Ionized Species at the Stagnation Region of a Blunt Body in Nonequilibrium Flow", GE TIS Report.
3. Blottner, F. G., "Nonequilibrium Laminar Boundary Layer Flow of Ionized Air", AIAA Journal, Vol. 2, No. 11, November 1964, pp. 1921-1927.
4. Lew, H. G., "Nonequilibrium Flow Over Stagnation Regions of Blunt Bodies in a Martian Atmosphere", GE Technical Memo, May 1967.
5. Power, R., private communication.

TABLE I - CHEMICAL REACTIONS

1. $O_2 + M = 2O + M$
2. $N_2 + M = 2N + M$
3. $NO + M = O + N + M$
4. $O + NO = N + O_2$
5. $O + N_2 = N + NO$
6. $O + N = NO^+ + e^-$
7. $N_2 + M = N_2^+ + e^- + M$
8. $N + N = N_2^+ + e^-$
9. $O_2 + N_2 = 2NO$
10. $CO_2 + O = CO + O_2$
11. $CO + O + M = CO_2 + M$
12. $OH + H_2 = H_2O + H$
13. $H + O_2 = OH + O$
14. $O + H_2 = OH + H$
15. $OH + OH = H_2O + O$
16. $H + H + M = H_2 + M$
17. $H + OH + M = H_2O + M$
18. $H + O + M = OH + M$
19. $C_2H_2 + 2O \rightarrow 2CO + H_2$
20. $CH_4 + 3O \rightarrow CO + 2H_2O$
21. $CH_4 + 2OH \rightarrow CO + 2H_2 + H_2O$
22. $C_2H_2 + O_2 \rightarrow 2CO + H_2$
23. $CH_4 + O_2 \rightarrow CO + H_2O + H_2$

Table I (cont'd)

24. $\text{CO} + \text{M} = \text{C} + \text{O} + \text{M}$
25. $\text{CO} + \text{N} = \text{CN} + \text{O}$
26. $\text{C}_2 + \text{O}_2 = 2\text{CO}$
27. $\text{Na} + \text{M} = \text{Na}^+ + \text{e}^- + \text{M}$
28. $\text{Na} + \text{e}^- = \text{Na}^+ + 2\text{e}^-$
29. $\text{Na}^+ + \text{O}^- = \text{Na} + \text{O}$
30. $\text{Na}^+ + \text{O}_2^- = \text{Na} + \text{O}_2$
31. $\text{Na} + \text{NO}^+ = \text{Na} + \text{NO}$
32. $\text{Na}^+ + \text{e}^- \rightarrow \text{Na} + h\nu$
33. $\text{O} + \text{e}^- \rightarrow \text{O}^- + h\nu$
34. $\text{O} + \text{e}^- + \text{M} = \text{O}^- + \text{M}$
35. $\text{O}_2 + \text{e}^- + \text{M} = \text{O}_2^- + \text{M}$
36. $\text{C}_2\text{F}_4 + \text{M} \rightarrow 2\text{CF}_2 + \text{M}$
37. $\text{C}_2\text{F}_4 + \text{O} \rightarrow \text{F}_2\text{CO} + \text{CF}_2$
38. $\text{CF}_2 + \text{O}_2 \rightarrow \text{CO} + 2\text{F} + \text{O}$
39. $\text{CF}_4 + \text{M} \rightarrow \text{CF}_2 + 2\text{F} + \text{M}$
40. $\text{F}_2\text{CO} + \text{M} \rightarrow \text{CO} + 2\text{F} + \text{M}$
41. $\text{F}_2 + \text{M} = 2\text{F} + \text{M}$
42. $\text{F}_2 + \text{e}^- = \text{F} + \text{F}^-$
43. $\text{F}^- + \text{M} = \text{F} + \text{e}^- + \text{M}$
44. $\text{F} + \text{e}^- \rightarrow \text{F}^- + h\nu$
45. $\text{CO} + \text{O} \rightarrow \text{CO}_2 + h\nu$

TABLE II - CHEMICAL RATE CONSTANTS

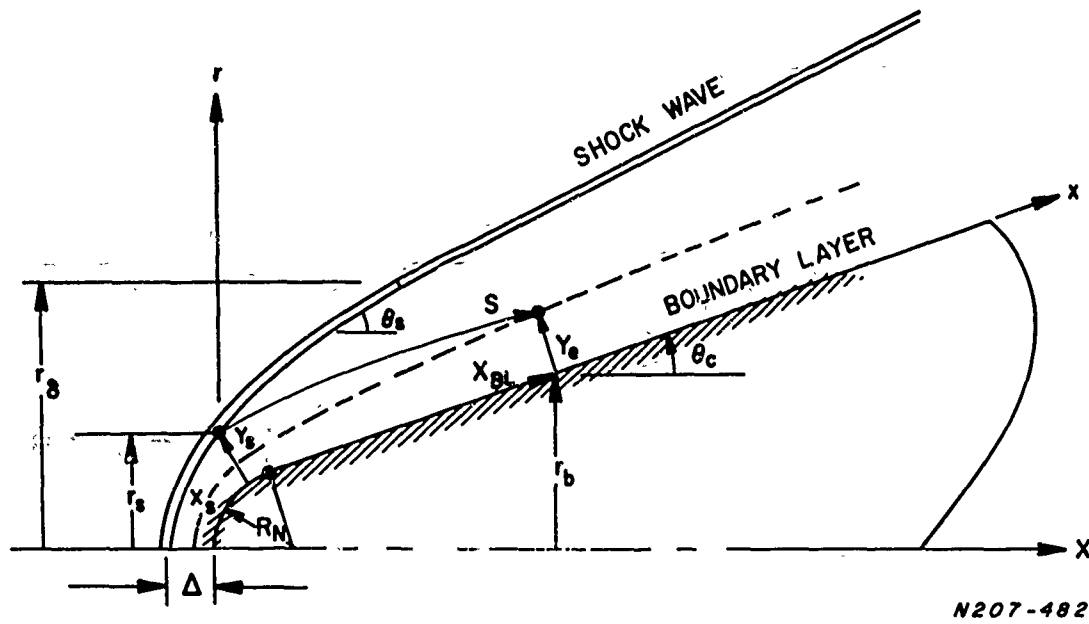
Rate Constant: $k = aT^b e^{-c/T}$, (d) = $\cdot 10^d$

Moles/cc, sec, $^{\circ}k$, and cal/gmol

<u>REACTION</u>	<u>FORWARD</u>			<u>BACKWARD</u>		
	<u>a</u>	<u>b</u>	<u>c</u>	<u>a</u>	<u>b</u>	<u>c</u>
1	.25 (+17)	- .5	.5938 (5)	.39 (15)	- .34	0
2	.2 (22)	-1.5	.113174 (6)	.18 (21)	-1.55	0
3	.55 (21)	-1.5	.75483 (5)	.26 (21)	-1.58	0
4	.32 (10)	1	.19676 (5)	.45 (11)	.85	.354 (4)
5	.68 (14)	0	.377 (5)	.22 (14)	- .05	0
6	.64 (10)	.5	.324 (5)	.64 (19)	- .89	0
7	.60225 (8)	.5	.181 (6)	.3627 (6)	-1	0
8	.463732 (9)	1.3	.678 (5)	.523958 (18)	- .2	0
9	.13 (26)	-2.62	.64664 (5)	.81675 (23)	-2.35	.43076 (5)
10	.6 (12)	0	.29 (5)	.6 (9)	0	.25 (5)
11	.5 (16)	0	.176 (4)	.109 (21)	- .58	.649 (5)
12	.63 (14)	0	.2969 (4)	.23 (13)	.01	.1041 (5)
13	.24 (15)	0	.8429 (4)	.198 (13)	.27	.491 (2)
14	.33 (13)	0	.3593 (4)	.107 (13)	.03	.2613 (4)
15	.76 (13)	0	.5032 (4)	.865 (14)	- .02	.8924 (4)
16	.2 (19)	-1	0	.143 (19)	- .82	.51952 (5)
17	.23 (22)	-1.5	0	.606 (22)	-1.31	.59393 (5)
18	.3 (15)	0	0	.696 (14)	.21	.50972 (5)

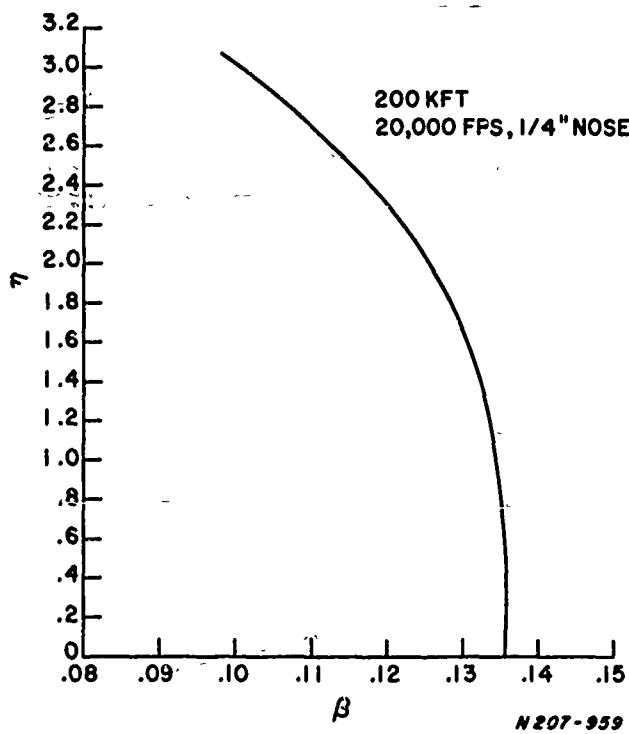
<u>REACTION</u>	<u>FORWARD</u>			<u>BACKWARD</u>		
	<u>a</u>	<u>b</u>	<u>c</u>	<u>a</u>	<u>b</u>	<u>c</u>
19	.15 (14)	0	0	0	0	0
20	.2 (14)	0	.345 (4)	0	0	0
21	.27 (14)	0	.3 (4)	0	0	0
22	.35 (18)	0	.34 (5)	0	0	0
23	.4 (15)	0	.275 (5)	0	0	0
24	.6 (16)	0	.29 (5)	.6 (9)	0	.25 (5)
25	.24 (13)	- .5	.46 (5)	.12 (12)	- .5	.53 (4)
26	.3 (14)	0	.37 (5)	.92 (12)	.72	.1633 (6)
27	.39 (7)	1.5	.597 (5)	.97 (15)	0	0
28	.39 (15)	.5	.597 (5)	.97 (23)	-1	0
29	.12 (18)	- .5	0	.4 (16)	- .5	.43 (5)
30	.12 (18)	- .5	0	.82 (17)	- .5	.545 (5)
31	.3 (14)	- .5	0	.92 (11)	0	.476 (5)
32	.12 (15)	- .75	0	0	0	0
33	.72 (9)	0	0	0	0	0
34	.11 (20)	- .5	0	.13 (13)	1	.17 (5)
35	.2 (19)	- .5	0	.12 (11)	1	.511 (4)
36	.782 (16)	.5	.28024 (5)	1	0	0
37	.6 (12)	0	0	1	0	0
38	.292 (11)	.5	.66828 (5)	1	0	0
39	.924 (15)	.5	.48130 (5)	1	0	0
40	.429 (12)	.5	.27967 (5)	1	0	0

<u>REACTION</u>	<u>FORWARD</u>			<u>BACKWARD</u>		
	<u>a</u>	<u>b</u>	<u>c</u>	<u>a</u>	<u>b</u>	<u>c</u>
41	.79 (13)	.2	.18475 (5)	.329 (13)	0	0
42	.33 (16)	0	0	.3 (8)	1.4	.21541 (5)
43	.3 (12)	.7	.40017 (5)	.136 (20)	- .9	0
44	.2 (10)	0	0	1	0	0
45	.2 (7)	0	.1610 (4)	1	0	0



N207-482

Figure 1. Blunt Conical Body



N207-959

Figure 2. Variation of Axial Pressure Gradient Across Layer

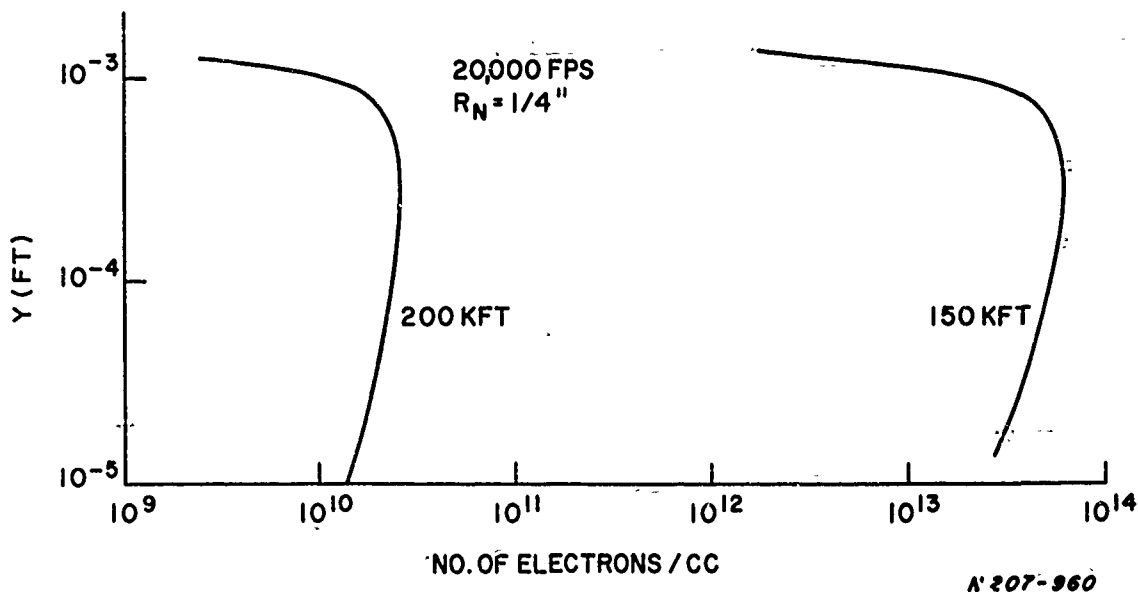


Figure 3. Electron Density Variation Across Viscous Layer for Variable β

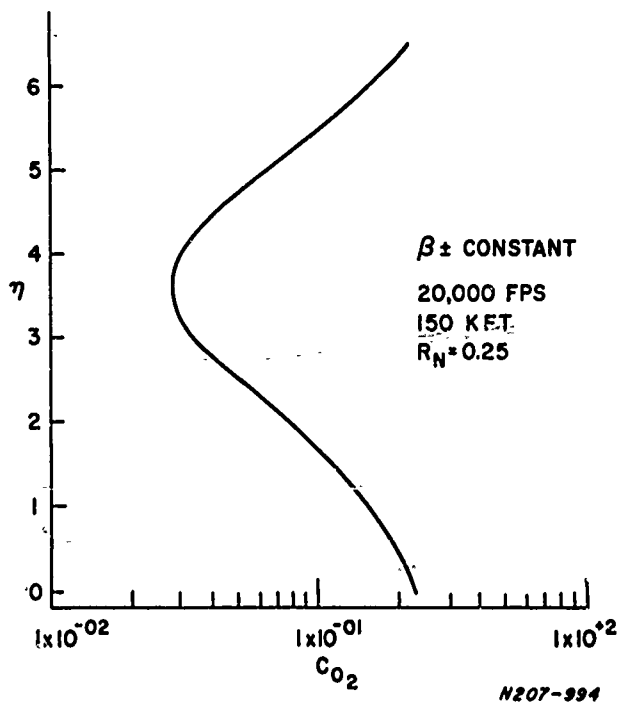


Figure 4. Oxygen Concentration, Stagnation Point

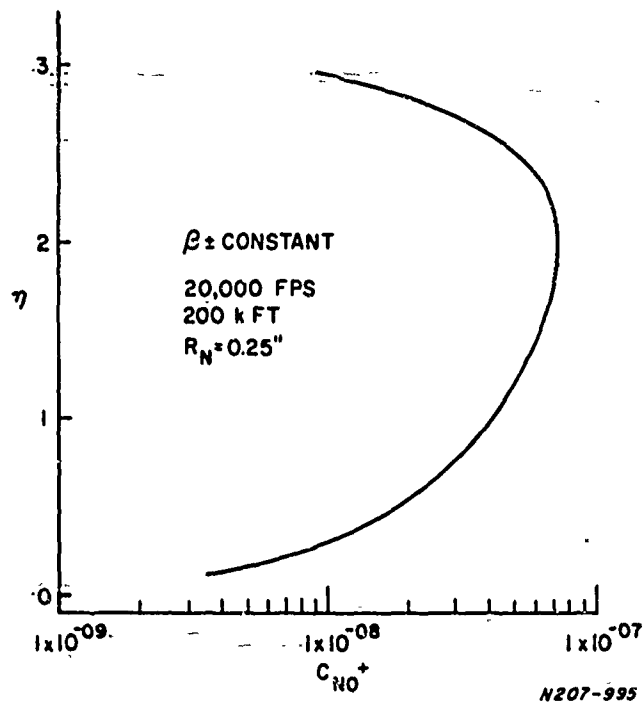


Figure 5. NO^+ , Stagnation Point

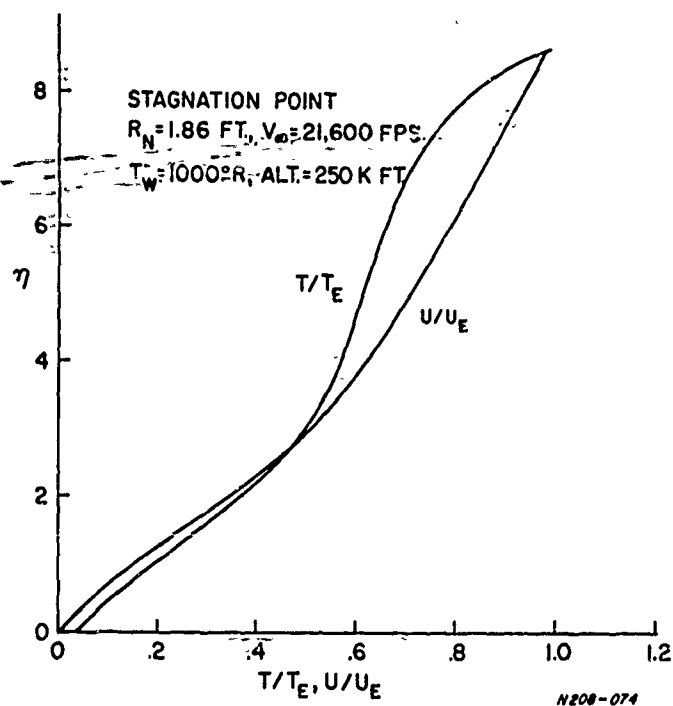


Figure 6. Temperature and Velocity Variation Across Viscous Layer, 250,000 ft.

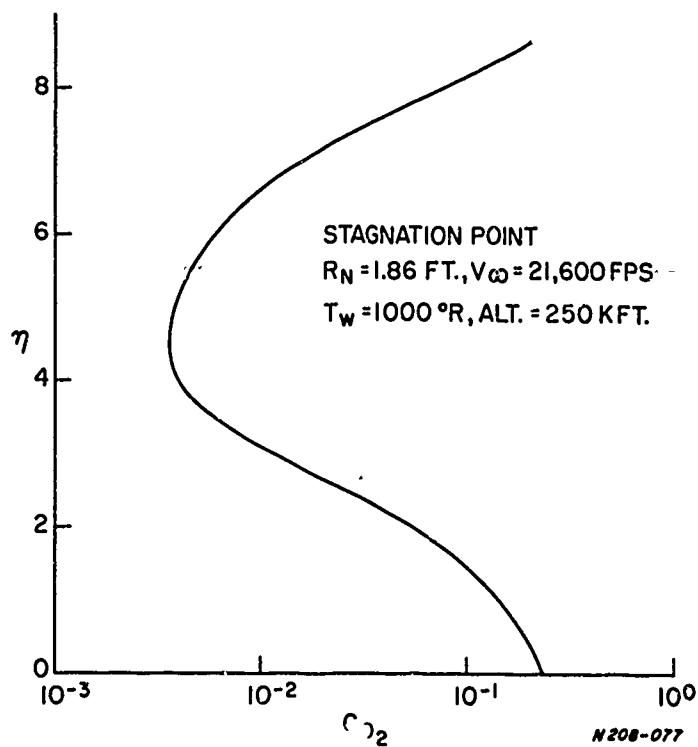


Figure 7. Mass Fraction of Oxygen Molecule Across the Viscous Layer, 250,000 ft.

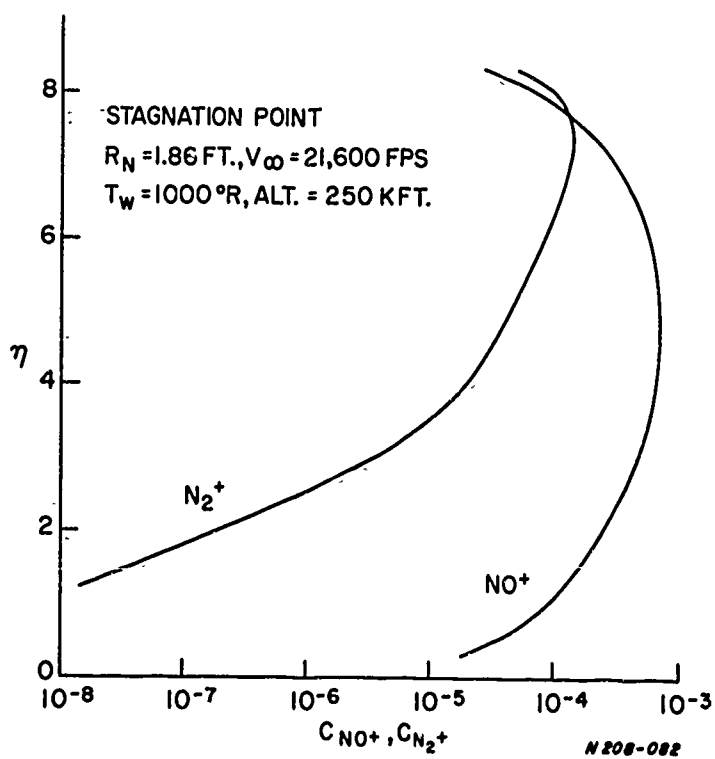


Figure 8. Positive Ion Distribution Across Viscous Layer, 250,000 ft.

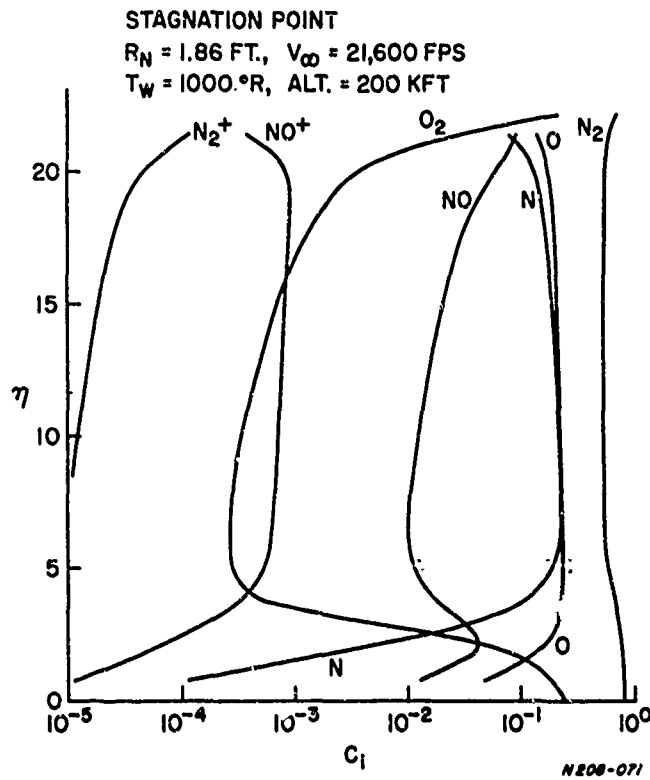


Figure 11. Species Distribution Across Viscous Layer, 200,000 ft.

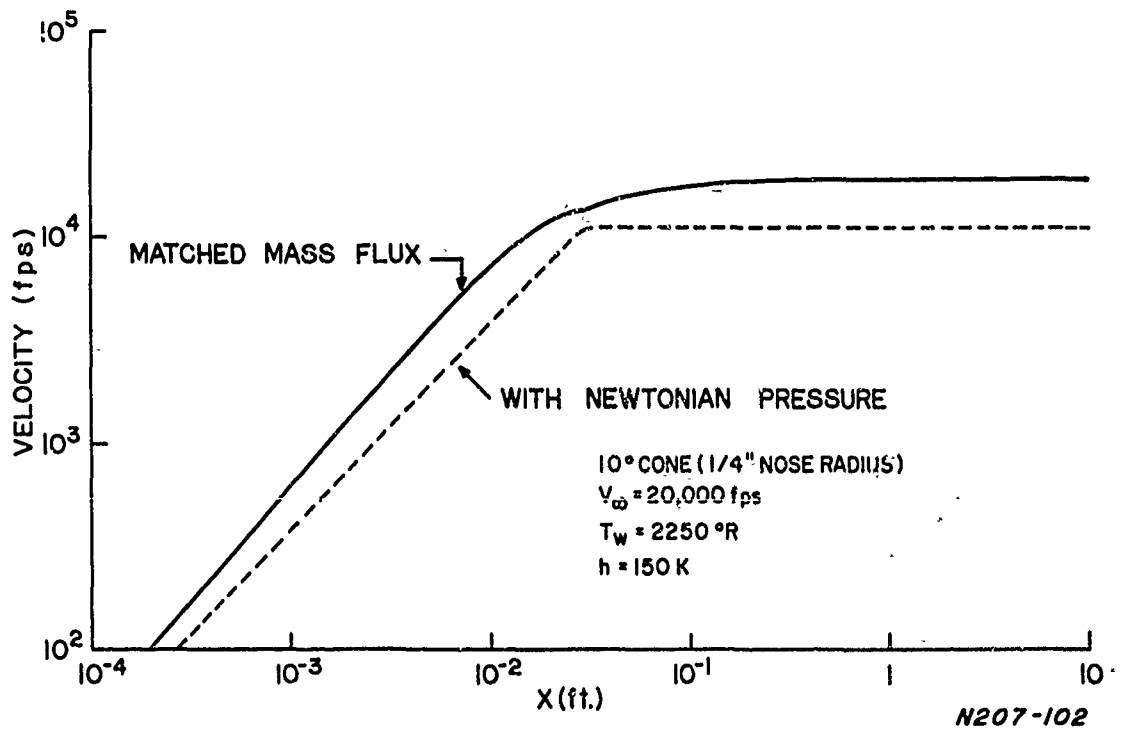


Figure 12. Velocity at Edge of Boundary Layer

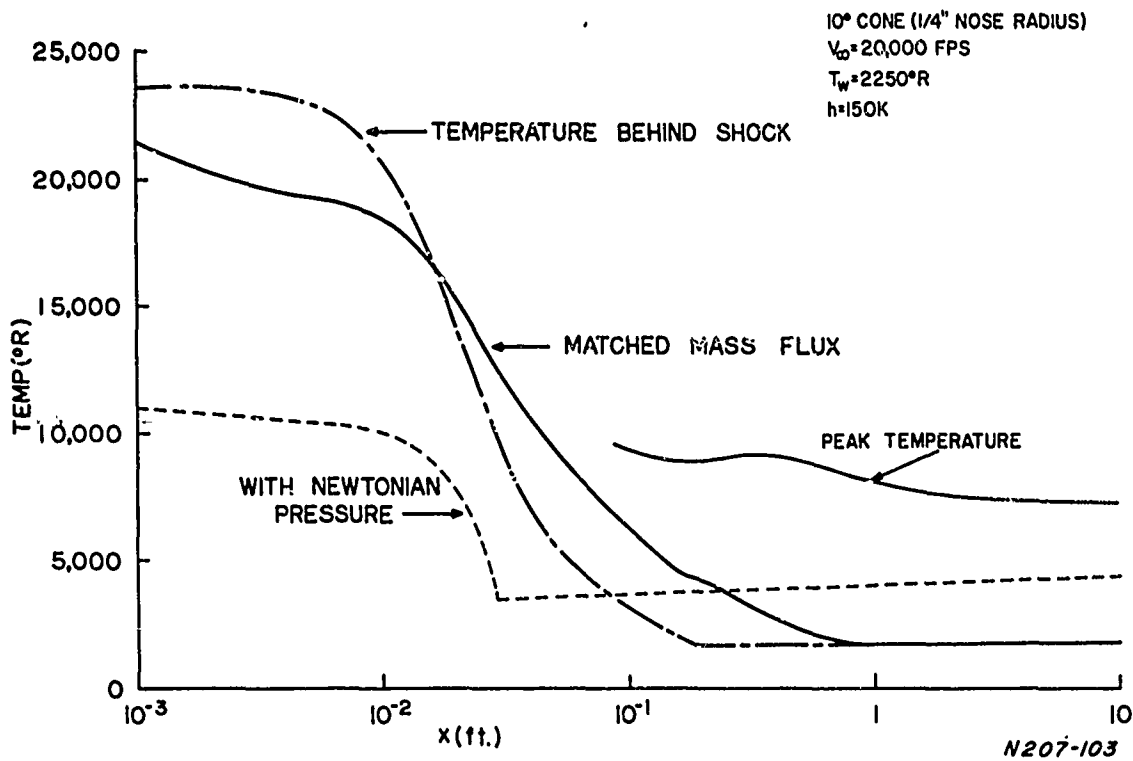


Figure 13. Temperature Along Body

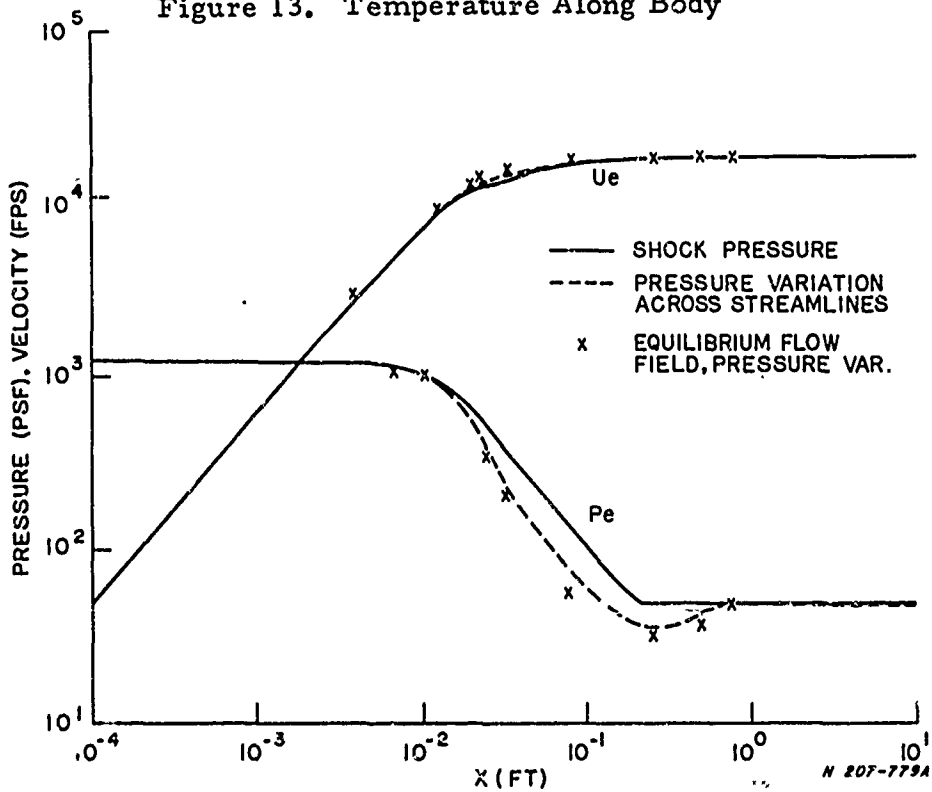


Figure 14. Pressure and Velocity Distribution Along Outer Edge of Boundary Layer

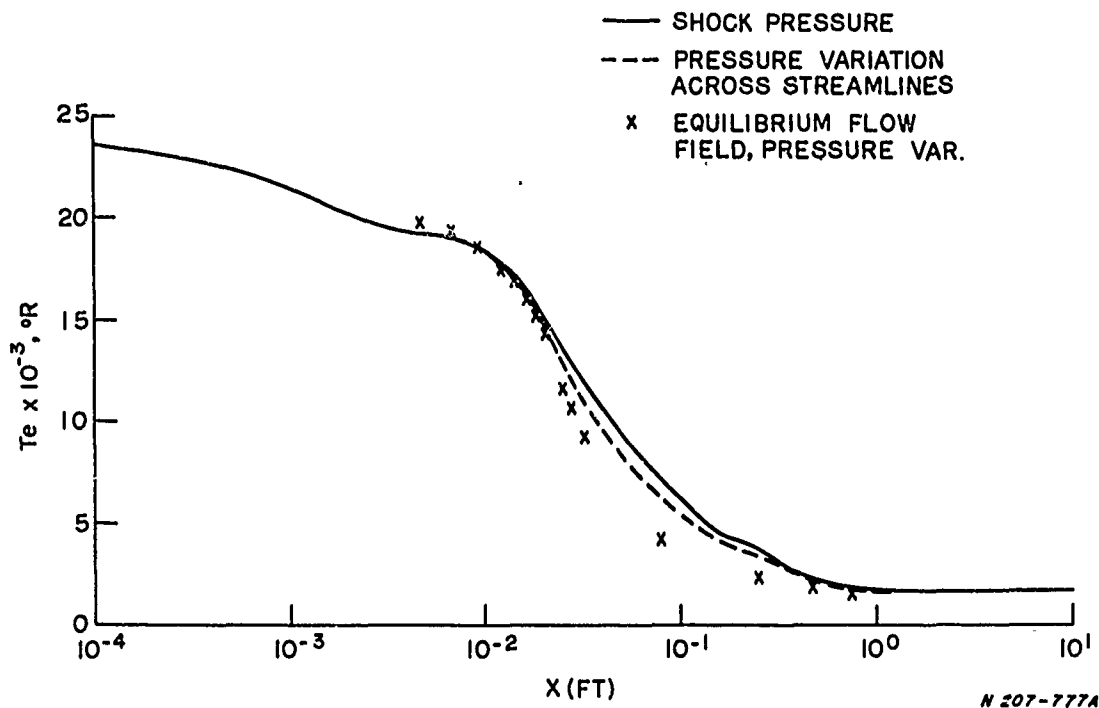


Figure 15. Temperature Distribution Along Outer Edge of Boundary Layer

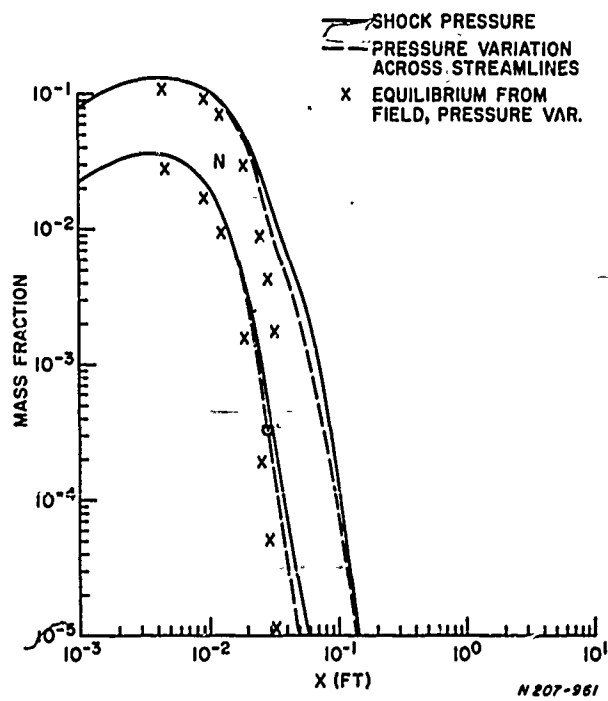


Figure 16. Atomic O and N Distribution Along Outer Edge of Boundary Layer

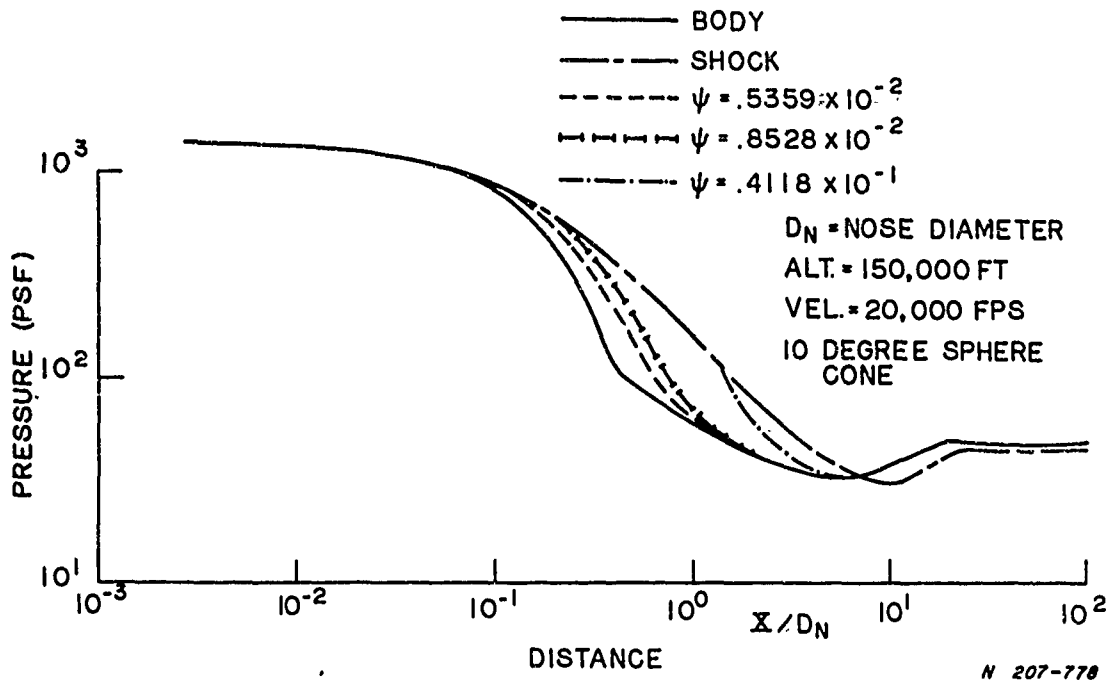


Figure 17. Pressure Distribution Along Inviscid Streamlines

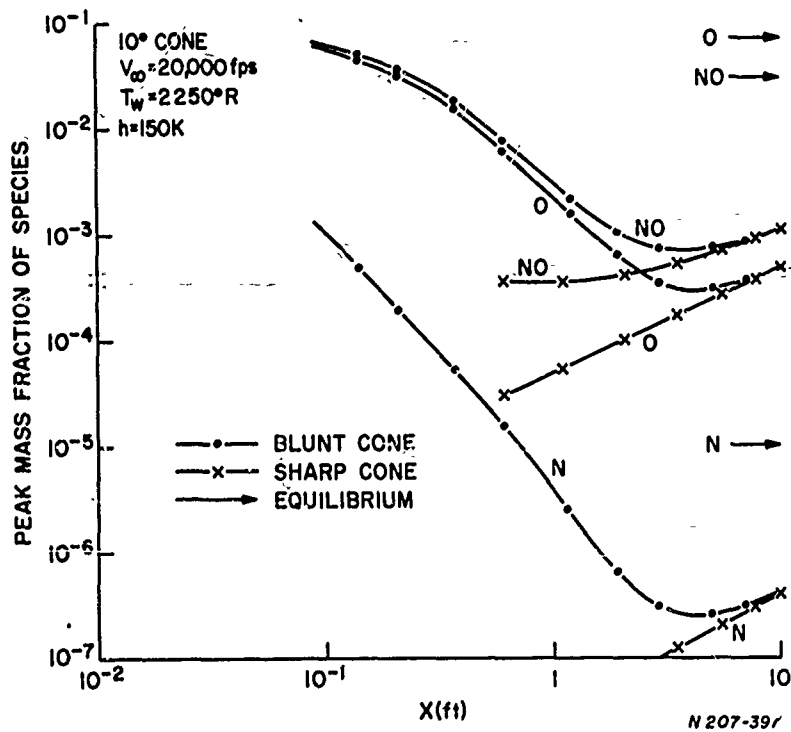


Figure 18. Peak Mass Fraction of Species Along Body

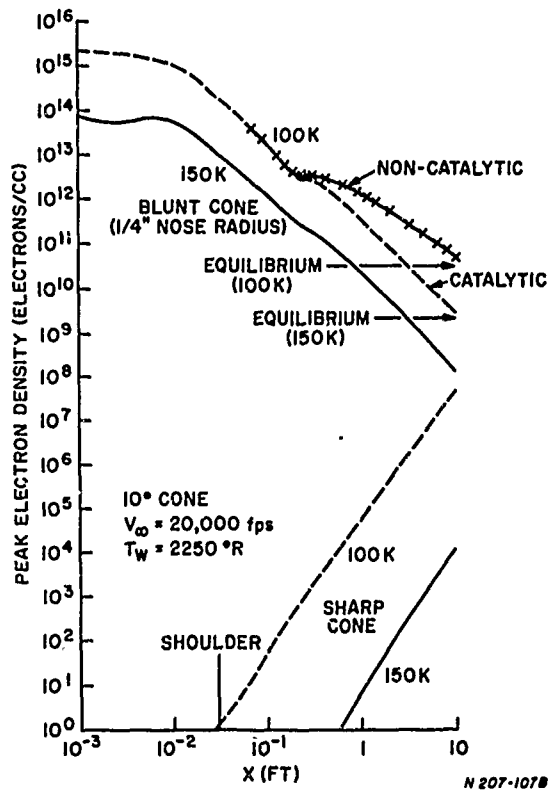


Figure 19. Peak Electron Density on Blunt Cones

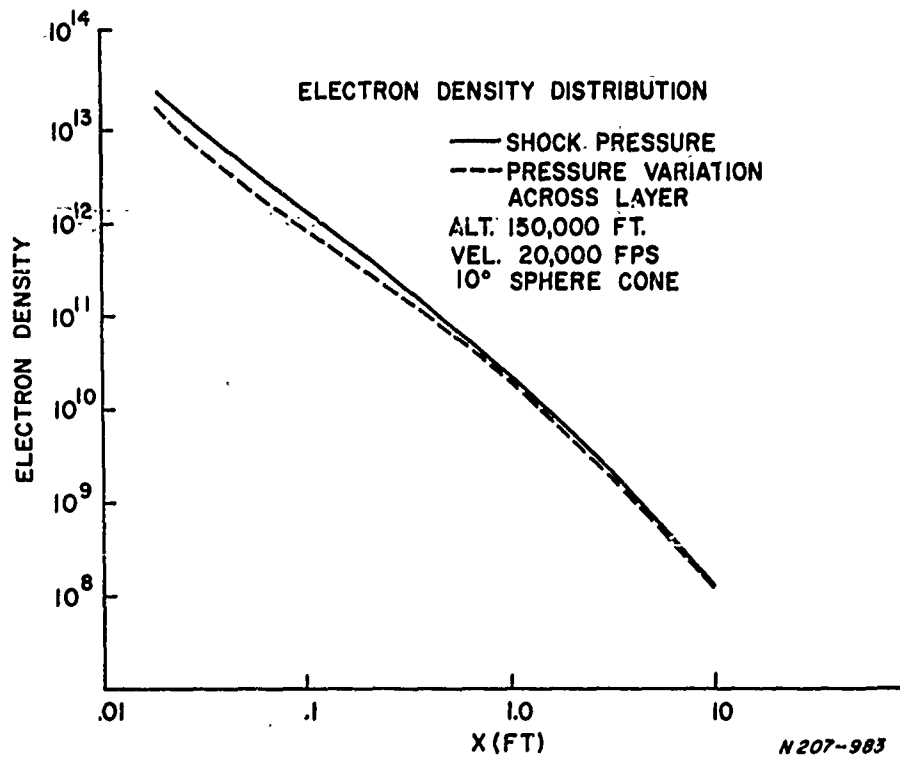


Figure 20. Maximum Electron Density Distribution

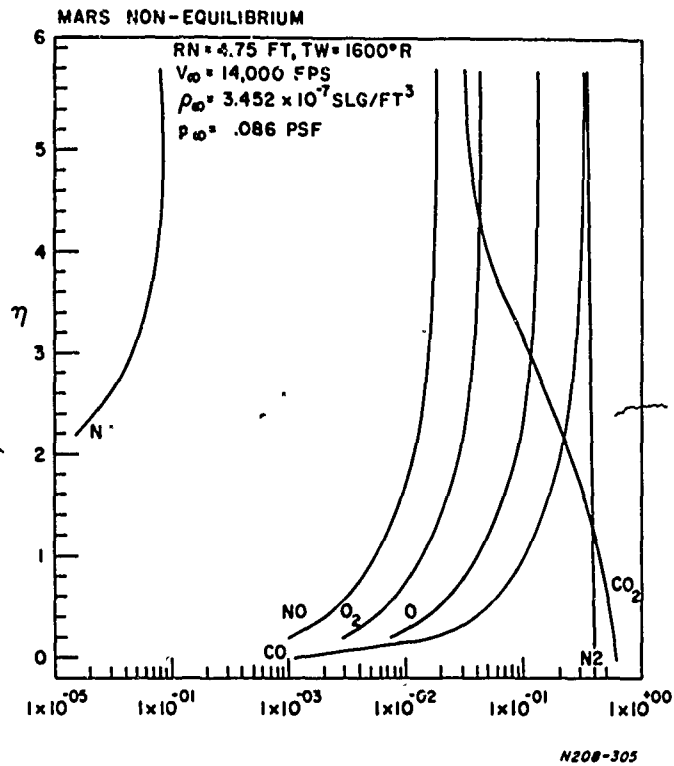


Figure 21. Mass Fraction of Species Across the Boundary Layer

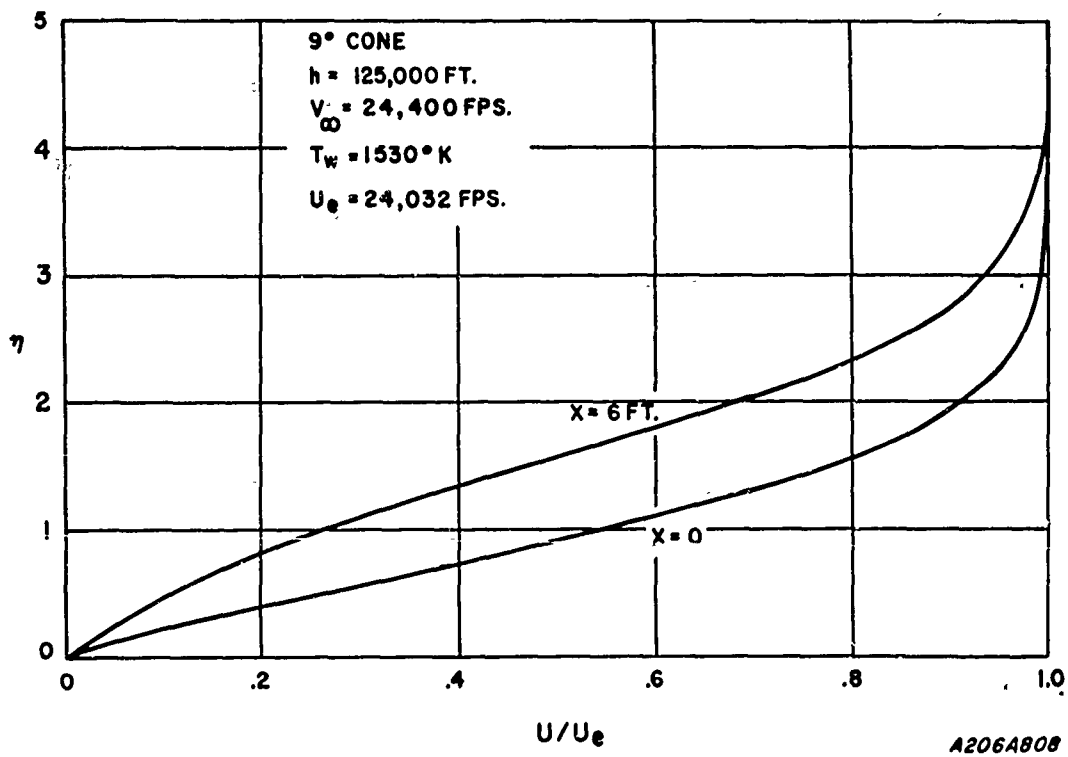


Figure 22. Velocity Profiles with Injection of Pyrolysis Gases

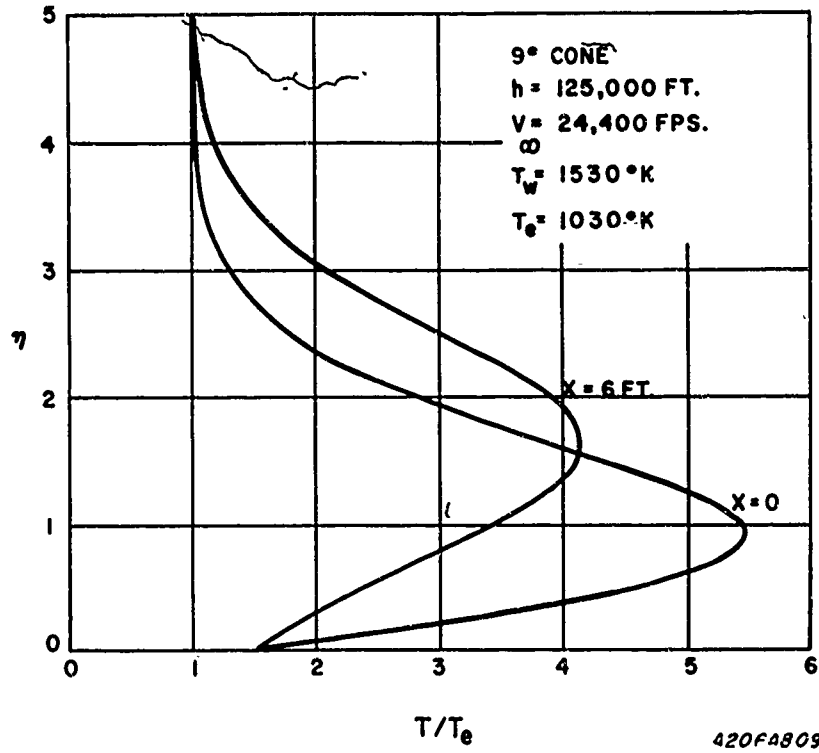


Figure 23. Temperature Profiles with Injection of Pyrolysis Gases

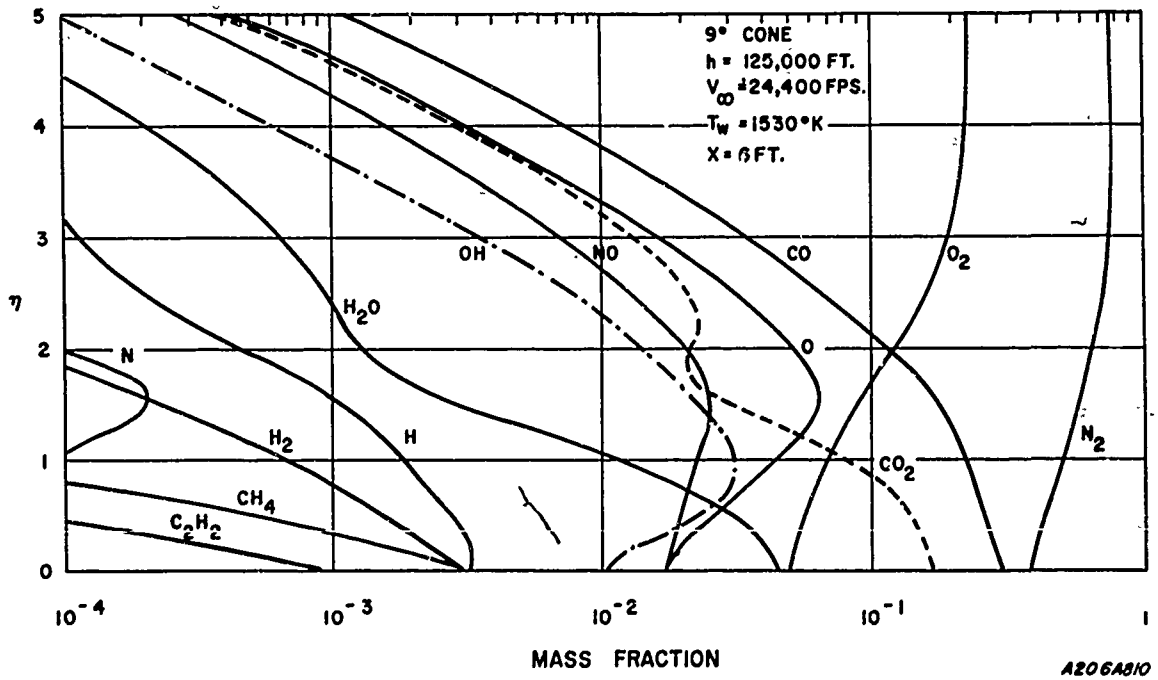


Figure 24. Mass Fraction Profiles with Injection of Pyrolysis Gases

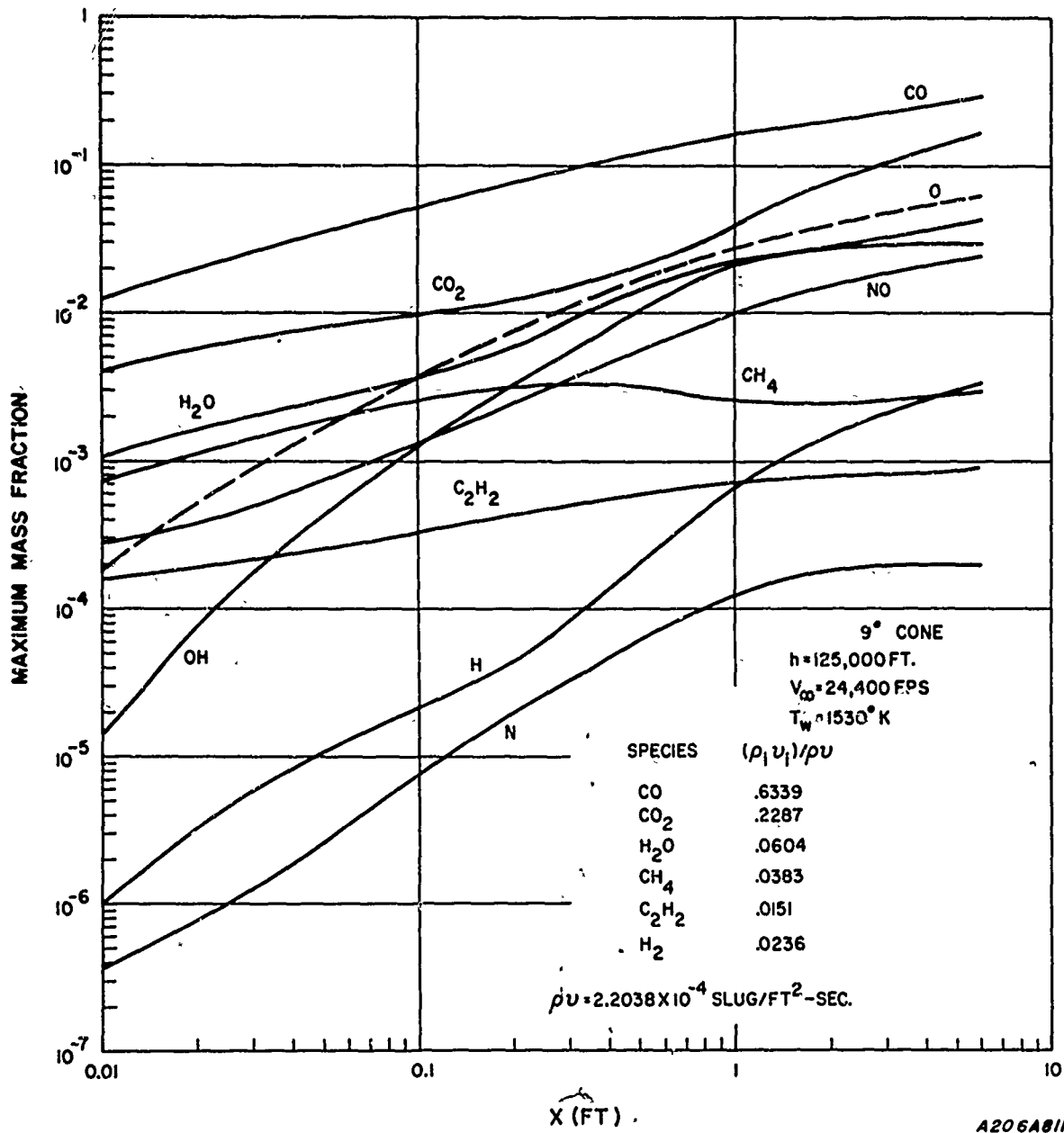


Figure 25. Maximum Mass Fraction Profiles With Injection of Pyrolysis Gases

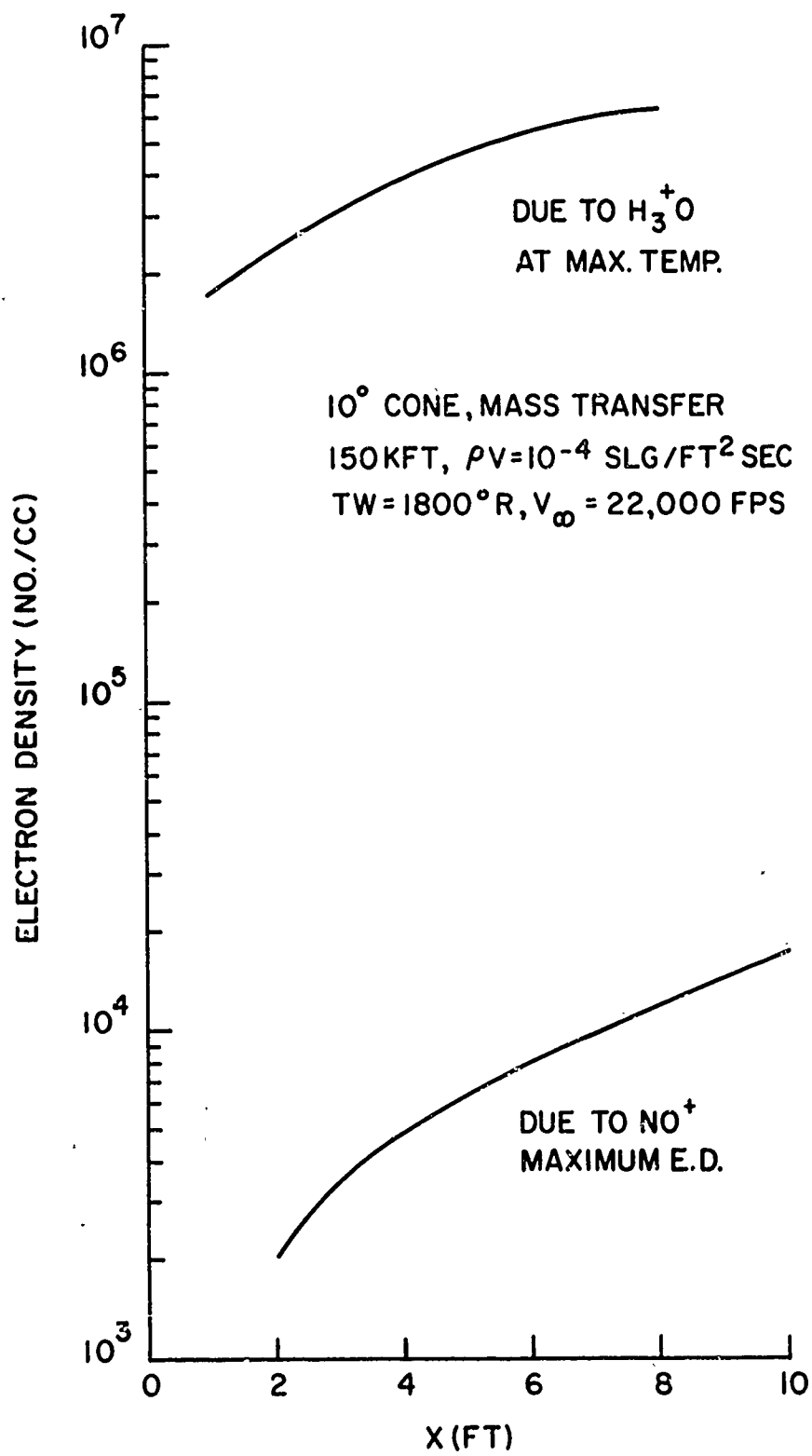


Figure 26. Electron Density for Hydrocarbon - Air Boundary Layer

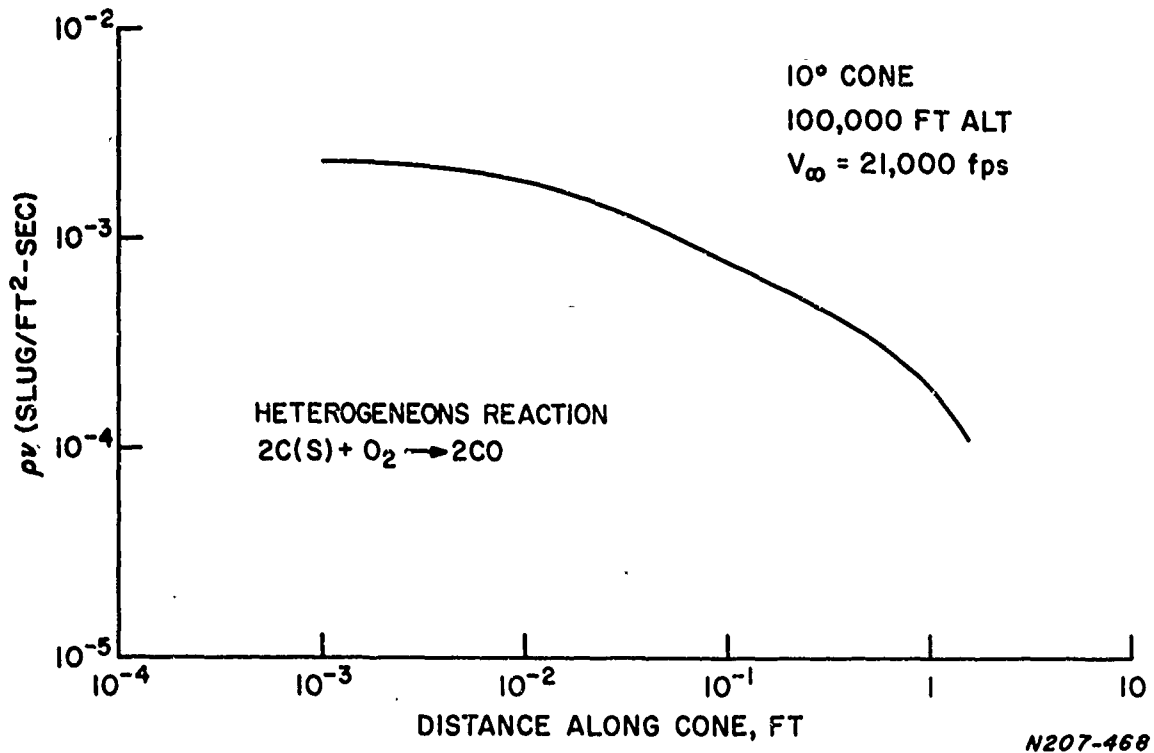


Figure 27. Mass Flux into the Boundary Layer for Graphite Oxidation

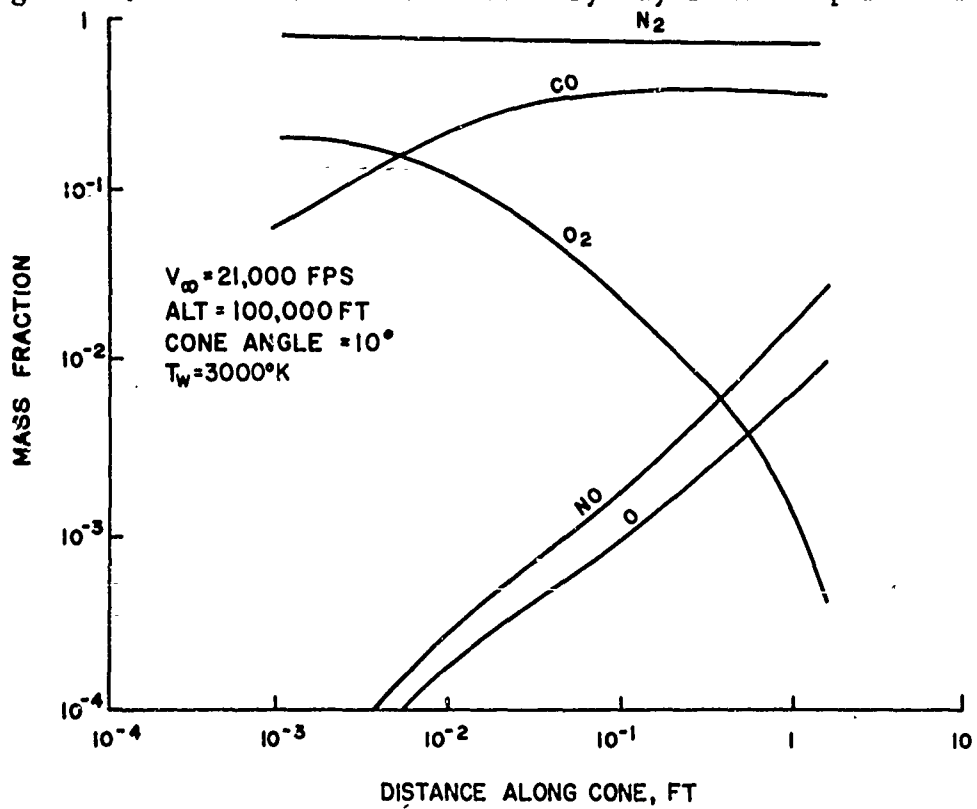


Figure 28. Mass Fraction of Species at Wall

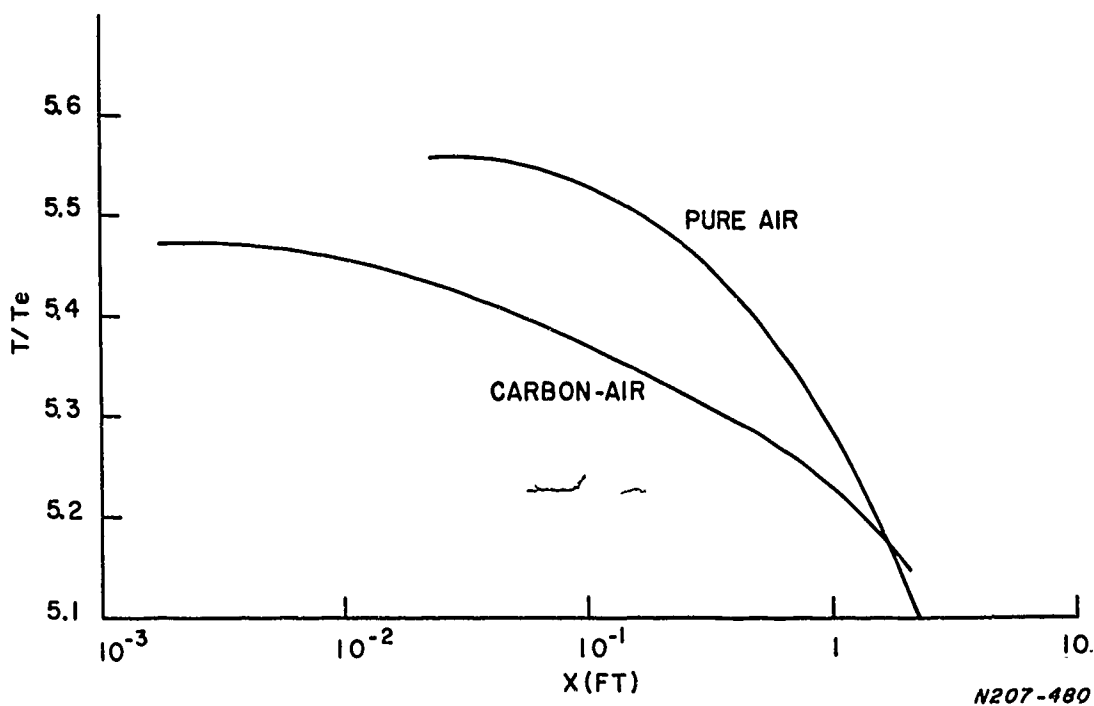


Figure 29. Maximum Temperature in the Boundary Layer

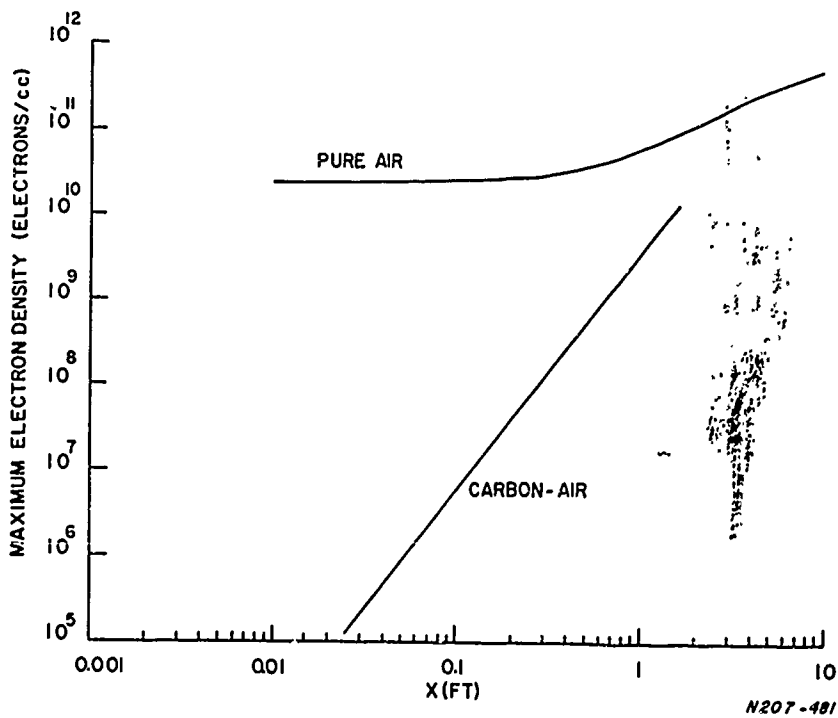
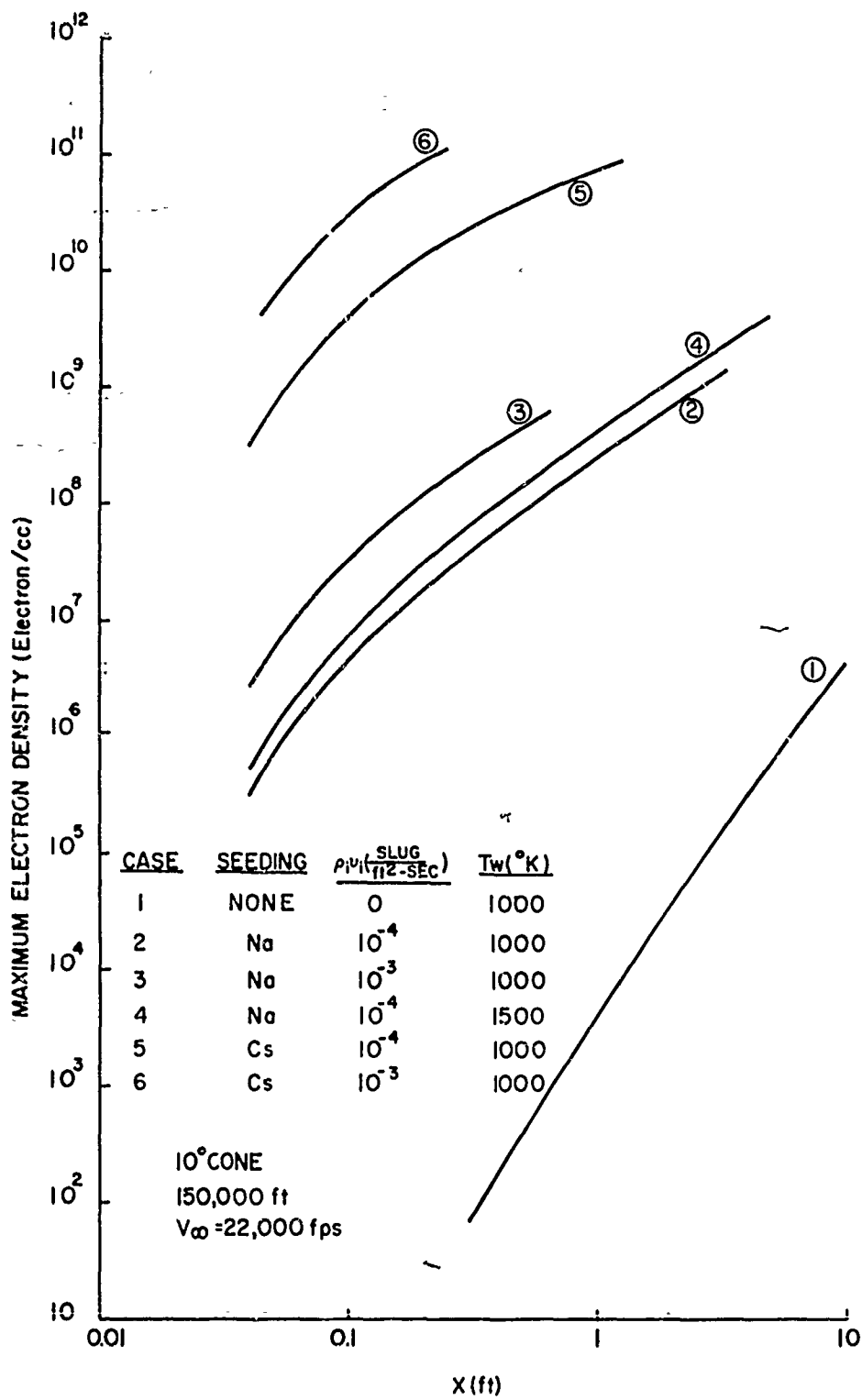


Figure 30. Maximum Electron Density



A205A004

Figure 31. Peak Electron Density with Seeding

SPACE SCIENCES LABORATORY
MISSILE AND SPACE DIVISION

GENERAL ELECTRIC

TECHNICAL INFORMATION SERIES

AUTHOR H. G. Lew	SUBJECT CLASSIFICATION Nonequilibrium Boundary Layer	NO. R67SD70
TITLE The Ionized Flow Field Over Re-Entry Bodies		DATE December 1967
		G. E. CLASS I
		GOV. CLASS Unclassified
REPRODUCIBLE COPY FILED AT MSD LIBRARY, DOCUMENTS LIBRARY UNIT, VALLEY FORGE SPACE TECHNOLOGY CENTER, KING OF PRUSSIA, PA.		NO. PAGES 52
SUMMARY The prediction of communication through the ionized flow field about a re-entry body requires the knowledge of the detailed distribution of electron density. Results are presented for obtaining the characteristics of the chemically reacting boundary layer and viscous layer with finite reaction rates on sharp and blunt conical re-entry vehicles with the inclusion of the effects of mass transfer from ablation products and surface reactions. It is found that the effect of a small bluntness at the nose creates a dominant number of electrons and these effects of a small nose radius on re-entry body characteristics and electron density are discussed and comparisons are made with those of a sharp cone. In addition, the results of this investigation (discussed herein) include the effects of alkali metal seeding, mass transfer of hydrocarbon ablation products, and catalytic surface characteristics on the electron density distributions.		
KEY WORDS Ionized Flows, Plasma Sheath, Communications, Wakes		

BY CUTTING OUT THIS RECTANGLE AND FOLDING ON THE CENTER LINE, THE ABOVE INFORMATION CAN BE FITTED INTO A STANDARD 8 1/2 X 11 FILE.

AUTHOR

H. G. Lew

H. G. Lew, Group Leader, Gas Dynamics

COUNTERSIGNED

S. M. Scala

S. M. Scala, Manager, Theoretical Fluid Physics Section